

Long-lived Searches of Vector-like Lepton and Its Accompanying Scalar at Colliders

Qing-Hong Cao,^{1,2,a} Jinhui Guo,^{3,b} Jia Liu,^{3,2,c} Yan Luo,^{3,d} and Xiao-Ping Wang^{4,5,e}

¹*School of Physics, Peking University, Beijing 100871, China*

²*Center for High Energy Physics, Peking University, Beijing 100871, China*

³*School of Physics and State Key Laboratory of Nuclear Physics and Technology, Peking University, Beijing 100871, China*

⁴*School of Physics, Beihang University, Beijing 100083, China*

⁵*Beijing Key Laboratory of Advanced Nuclear Materials and Physics, Beihang University, Beijing 100191, China*

Abstract

Recently, the vector-like leptons (VLLs) as a simple extension to the standard model (SM) have attracted widespread attention both in theory and experiments. The present collider searches mainly focus on the studies of their prompt decays, which prefer a relatively large coupling. In this paper, we concentrate on searches for long-lived signatures of the singlet VLLs F or their accompanying scalar particles ϕ both in the hadronic and electronic colliders. The long-lived signatures are naturally induced from small chiral mass mixing between VLLs and SM leptons. Two specific models distinguished by whether the VLLs couple to scalar particles are introduced to realize the aforementioned features. For long-lived VLLs case, we find that with the kink track method the sensitivities at future HL-LHC with $\sqrt{s} = 13$ TeV can reach the regions for VLL mass $m_F \in [200, 950]$ GeV and the mass mixing parameter $\theta_L \in [10^{-10}, 10^{-7}]$. For the long-lived accompanying scalar particle case, by fixing VLLs or scalar mass, or the mass ratio between VLL and the accompanying scalar, we explore the projected sensitivities through the time delay and displaced vertex strategies, which can probe the regions for $m_F \in [200, 1200]$ GeV and coupling $y\theta_L \in [10^{-11}, 10^{-6}]$. Furthermore, we also explore the long-lived accompanying scalars at the future CEPC provided that the VLLs can couple to the SM first-generation leptons. We find that CEPC has good performances for $m_\phi < 70$ GeV and $m_F < 1000$ GeV. These long-lived searches are complementary to previous studies, which opens the door towards the smaller coupling regions.

^a qinghongcao@pku.edu.cn

^b guojh23@pku.edu.cn

^c jialiu@pku.edu.cn

^d ly23@stu.pku.edu.cn

^e hcwangxiaoping@buaa.edu.cn

CONTENTS

I. Introduction	2
II. The Models	4
A. Vector-like Lepton Scenario (VLLS)	5
B. Vector-like Lepton with Scalar (VLLWS)	6
III. Existing Constraints	7
A. Constraints from Heavy Stable Charged Particles Searches	8
B. Constraints from Multilepton Searches at LHC	8
C. Constraints from Lepton Flavor Violations	10
1. LFV for VLLS	11
2. LFV for VLLWS	13
D. Constraints from $g - 2$	15
IV. Long-lived particle signatures at Colliders	17
A. Long-lived vector-like lepton	18
B. Long-lived scalar particle	20
1. Displaced vertex search	21
2. Time delay search	22
C. Search for long-lived scalars at future CEPC	24
V. Conclusions	27
VI. Acknowledgments	28
References	29

I. INTRODUCTION

Vector-like fermion (VLF) is one of the simplest extensions of the Standard Model (SM), which transforms as a non-chiral representation of SM gauge group and can arise in e.g. string-theory models or grand unified theories (GUTs), beyond three-generation fermions [1]. Heavy VLFs can realize the flavor democracy [2], and there have been many searches for vector-like quark for

decades, both by Tevatron [3, 4] and Large Hadron Collider (LHC) [5–9]. If the VLFs only couple to the SM leptons, they are usually referred to as vector-like leptons (VLLs), and have been paid more attention recently. They are often classified by their coupled SM lepton generation, where they possess the same quantum numbers as the SM leptons.

Conventional searches for these particles usually focus on the associated production or pair production followed by the prompt decays of VLLs, such as the searches for VLL doublet coupled to the third-generation conducted by the ATLAS and CMS [10–13]. Collider phenomenology research on different decay modes of VLLs has been conducted [1, 14–17]. Additionally, there is a dedicated study that delves into a model featuring a VLL doublet and scalars, which has the capability to generate the requisite baryon asymmetry [18]. Moreover, investigations have delved into the searches for $SU(2)_L$ singlet VLLs with a small mass mixing to SM leptons, originating from the Yukawa coupling to the Higgs field. These searches have been studied at the LHC and proposed for future $e^-e^+/\mu^+\mu^-$ colliders [19–22]. Furthermore, other noteworthy discussions regarding VLLs in the context of Higgs physics and new physics have been explored in Refs. [23–45].

It is important to highlight that previous VLL searches have predominantly concentrated on the production of VLLs and their subsequent prompt decays, with an emphasis on strong couplings during their investigations. In contrast, recent research endeavors have explored alternative aspects of VLLs and their interactions. For instance, a study has examined the interplay between an inert Higgs doublet dark matter and a VLL triplet, specifically considering the potential for displaced vertices signals detectable at the MATHUSLA detector [46]. Furthermore, another recent investigation delved into a model featuring a weak-singlet VLL denoted as τ' and a complex scalar, studying the phenomenology of long-lived pseudoscalar signals at the LHC [47]. In their model, the complex scalar possesses a non-zero vacuum expectation value (vev), resulting in the mass of pseudoscalar being suppressed to a few GeV, different from our model, the mass of the scalar can reach several hundred GeV. Furthermore, our research primarily centers on cases where VLLs couple with either electrons or muons, and we additionally explore scenarios involving long-lived weak-singlet VLLs.

In our study, we place significant emphasis on the long-lived signatures of VLLs and their accompanying scalar particles, as this aspect is both crucial and complementary. These long-lived features often involve tiny couplings, which prove invaluable in addressing issues related to lepton flavor violations (LFV). To illustrate this, we present two models featuring an $SU(2)_L$ singlet

charged VLL, denoted as F^\pm , which undergoes mixing with SM leptons via direct mass mixing. We propose a search strategy for these novel particles based on their long-lived signatures. In the first model, we seek long-lived VLLs F^\pm with a kink track signature, where the production of F^-F^+ pairs occurs through the Drell-Yan process, followed by their long-lived subsequent decays to $Z\ell^\pm$ or $W^\pm\nu_\ell$. In the second model, we introduce a long-lived accompanying scalar particle coupled to both F^\pm and SM leptons via a substantial Yukawa interaction, and we explore its detection using time delay and displaced vertex signatures. Our first chosen search platform is the high-luminosity LHC (HL-LHC), a traditional facility for exploring heavy new particles. These searches extend the parameter space set by ATLAS and CMS, opening new possibilities for discovery.

Moreover, in contrast to the first model, the second model, despite its heavier mass, holds the exploration potential through the t channel production at future e^-e^+ colliders, especially when VLLs interact with electrons. To exemplify this, we consider the Circular Electron Positron Collider (CEPC) as an illustrative case. By examining the displaced vertex signatures associated with the scalar particles, CEPC exhibits excellent sensitivity, particularly in lighter mass regions, thanks to its pristine experimental conditions and lower center-of-mass energy.

We organize the paper as follows. In section II, we describe the $SU(2)_L$ singlet VLL models with singlet scalar or without scalar, respectively, and their possible decay channels. In section III, we discuss the existing constraints from collider searches, LFV processes, and lepton $g-2$ measurements. In section IV, we discuss the long-lived particle (LLP) signatures and their detection at the HL-LHC and CEPC. In section V, we conclude.

II. THE MODELS

We expand SM with an extra $SU(2)_L$ singlet VLL F^\pm and a real scalar singlet ϕ , and their SM gauge group property are listed in Tab. I.

Gauge Group	Fermion Field (F^\pm)	Scalar Fields (ϕ)
$SU(2)_L \times U(1)_Y$	(1, -2)	(1, 0)

TABLE I. Gauge charges of new particles and relevant SM particles in SM groups.

In the following subsections, we discuss two scenarios: one with only the VLL F^\pm and another with both the VLL F^\pm and the scalar ϕ .

A. Vector-like Lepton Scenario (VLLS)

The effective Lagrangian related to F^\pm reads as

$$\mathcal{L}_{\text{eff}}^F \supset \bar{F}^0 iD_\mu \gamma^\mu F^0 + \bar{L}^0 iD_\mu \gamma^\mu L^0 + \bar{\ell}_R^0 iD_\mu \gamma^\mu \ell_R^0 - m_F^0 \bar{F}^0 F^0 - m_\ell^0 \bar{\ell}^0 \ell^0 - (\delta \bar{F}_L^0 \ell_R^0 + \text{h.c.}), \quad (1)$$

where the covariant derivative $D_\mu = \partial_\mu - ig' \frac{Y}{2} B_\mu - ig T^i W_\mu^i$, B_μ and W_μ^i represent the gauge fields for the SM $U(1)_Y$ and $SU(2)_L$ groups, respectively. The constants g' and g are their associated coupling constants. Furthermore, ℓ denotes charged lepton singlet, and L represents weak isospin doublets. All fields with a subscript '0' refer to interaction-eigenstates. Although it is possible for the Higgs boson to have a Yukawa coupling to SM leptons of the form $y' \bar{L} H F_R$, we neglect this possibility for long-lived particle studies because the F will decay promptly into an SM Higgs boson unless y' is very small. The mass of the VLL is primarily determined by its mass term, with a small correction introduced by the δ term. The mass part of Eq. (1) can be written as

$$\mathcal{L}_{\text{mass}}^F = (\bar{F}_L^0, \bar{\ell}_L^0) \begin{pmatrix} m_F^0 & \delta \\ 0 & m_\ell^0 \end{pmatrix} \begin{pmatrix} F_R^0 \\ \ell_R^0 \end{pmatrix} = (\bar{F}_L^0, \bar{\ell}_L^0) M \begin{pmatrix} F_R^0 \\ \ell_R^0 \end{pmatrix} = (\bar{F}_L, \bar{\ell}_L) U_L M U_R^\dagger \begin{pmatrix} F_R \\ \ell_R \end{pmatrix}, \quad (2)$$

where the unitary matrices are introduced to diagonalize the mass matrix

$$U_L M U_R^\dagger = \text{diag}(m_F, m_\ell), \quad (3)$$

and obtain the mass eigenstates F and ℓ . While the unitary matrices can be parameterized as

$$U_L = \begin{pmatrix} \cos \theta_L & -\sin \theta_L \\ \sin \theta_L & \cos \theta_L \end{pmatrix}, U_R = \begin{pmatrix} \cos \theta_R & -\sin \theta_R \\ \sin \theta_R & \cos \theta_R \end{pmatrix}, \quad (4)$$

with

$$\begin{aligned} \tan \theta_R &= -\frac{2m_F^0 \delta}{(m_F^0)^2 - (m_\ell^0)^2 - \delta^2 + \sqrt{((m_F^0)^2 - (m_\ell^0)^2 + \delta^2)^2 + 4(m_\ell^0)^2 \delta^2}} \simeq -\frac{\delta}{m_F^0}, \\ \tan \theta_L &= -\frac{2m_\ell^0 \delta}{(m_F^0)^2 - (m_\ell^0)^2 + \delta^2 + \sqrt{((m_F^0)^2 - (m_\ell^0)^2 + \delta^2)^2 + 4(m_\ell^0)^2 \delta^2}} \simeq -\frac{m_\ell^0 \delta}{(m_F^0)^2} \simeq \frac{m_\ell^0}{m_F^0} \tan \theta_R, \end{aligned} \quad (5)$$

The approximation is valid in the limits where $m_F^0 \gg m_\ell^0$, δ . Due to this hierarchy, the mixing angle θ_L is significantly suppressed by an additional factor of m_ℓ^0/m_F^0 in comparison to θ_R . This is a natural outcome as we introduce a heavy VLL, with the same gauge charge as the right-handed SM fermion. Thus, its mixing with right-handed fermions is considerably more straightforward

than with the left-handed counterparts. Consequently, we can establish $|\theta_L| \ll |\theta_R| \ll 1$. We also can simplify the mass eigenvalues

$$m_F \simeq m_F^0 + \frac{\delta^2}{2m_F^0} \simeq m_F^0 \quad (6)$$

$$m_\ell \simeq m_\ell^0 \left(1 - \frac{1}{2} \left(\frac{\delta}{m_F^0} \right)^2 \right). \quad (7)$$

To the lowest order of $\theta_L(\theta_R)$, the Lagrangian (1) in the mass eigenstates can be expressed as

$$\begin{aligned} \mathcal{L}_{\text{eff}}^F \supset & i\bar{F}\gamma^\mu\partial_\mu F + i\bar{\ell}\gamma^\mu\partial_\mu\ell - m_F\bar{F}F - m_\ell\bar{\ell}\ell \\ & - \frac{g}{2} \left(W_\mu^3(\bar{\ell}_L\gamma^\mu\ell_L - \theta_L\bar{F}_L\gamma^\mu\ell_L - \theta_L\bar{\ell}_L\gamma^\mu F_L) + (W_\mu^1 - iW_\mu^2)(-\theta_L\bar{\nu}_L\gamma^\mu F_L + \bar{\nu}_L\gamma^\mu\ell_L) + \text{h.c.} \right) \\ & - g'B_\mu \left(\bar{F}\gamma^\mu F + \frac{1}{2}\bar{\ell}_L\gamma^\mu\ell_L + \bar{\ell}_R\gamma^\mu\ell_R + \frac{\theta_L}{2}\bar{F}_L\gamma^\mu\ell_L + \frac{\theta_L}{2}\bar{\ell}_L\gamma^\mu F_L \right) \\ \supset & \bar{F}(i\partial_\mu - eA_\mu + e\tan\theta_W Z_\mu)\gamma^\mu F - m_F\bar{F}F - m_\ell\bar{\ell}\ell \\ & + \frac{1}{2} \frac{e}{\sin\theta_W \cos\theta_W} \theta_L Z_\mu (\bar{F}_L\gamma^\mu\ell_L + \text{h.c.}) - \frac{e}{\sqrt{2}\sin\theta_W} \theta_L (W_\mu^+ \bar{\nu}_L\gamma^\mu F_L + \text{h.c.}), \end{aligned} \quad (8)$$

where θ_W is the Weinberg angle. As expected in the last line, only the left-handed interactions between F and ℓ or ν exist due to the chiral mass mixing in Eq. (1), which also allow two decay channels for massive F . For $m_F > m_W, m_Z$, the corresponding decay width of F can be deduced to

$$\Gamma(F^\pm \rightarrow \nu_\ell W^\pm) = \frac{\theta_L^2 g_W^2 (m_F^2 - m_W^2)^2 (m_F^2 + 2m_W^2)}{64\pi m_F^3 m_W^2}, \quad (9)$$

$$\Gamma(F^\pm \rightarrow \ell^\pm Z) = \frac{\theta_L^2 g_Z^2 (m_F^2 - m_Z^2)^2 (m_F^2 + 2m_Z^2)}{64\pi m_F^3 m_Z^2}. \quad (10)$$

which is in the limit of $m_\ell \ll m_F$. As the decay width is proportional to the tiny θ_L^2 , F^\pm can be a long-lived charged particle candidate in collider detection, where it can imprint peculiar tracks.

B. Vector-like Lepton with Scalar (VLLWS)

If we add another real scalar singlet ϕ on the basis of F , an effective Yukawa interaction is added to Lagrangian (1),

$$\begin{aligned} \mathcal{L}_{\text{int}}^\phi \supset & -y\phi\bar{F}_L^0\ell_R^0 + \text{h.c.} \\ \simeq & -y\phi \left(\bar{F}_L\ell_R + \bar{\ell}_R F_L + \theta_R\bar{F}F - \theta_L\bar{\ell}\ell \right), \end{aligned} \quad (11)$$

where we only keep the lowest order of rotation angles $\theta_{L/R}$, and y is the Yukawa coupling constant. There are four free parameters in this scenario

$$\{m_F, m_\phi, y, \theta_L\}, \quad (12)$$

where θ_R is fixed by $\theta_R \approx \theta_L m_F / m_\ell$. We choose to treat θ_L as a free parameter instead of δ or θ_R , because it is more directly connected to the lifetime of LLP. In our study, we focus on the parameter space of $m_F > m_\phi \gg m_\ell$, and $m_F > 200$ GeV is set to avoid constraints from multilepton and Z boson searches, which will be discussed in Sec. III. We choose sizeable y to make F decay promptly so that ϕ is the only LLP in this scenario, but its value is bound to ensure safety from the measurements of LFVs, which will be discussed in Sec III.

In this scenario, the decay widths of the VLL $\Gamma(F^\pm \rightarrow \phi \ell^\pm)$ and the scalar $\Gamma(\phi \rightarrow \ell^+ \ell^-)$ are given by

$$\begin{aligned} \Gamma(F^\pm \rightarrow \phi \ell^\pm) &= \frac{y^2(m_F^2 + m_\ell^2 - m_\phi^2) \sqrt{\lambda(m_F^2, m_\phi^2, m_\ell^2)}}{32\pi m_F^3}, \\ \Gamma(\phi \rightarrow \ell^+ \ell^-) &= \frac{(y\theta_L)^2 m_\phi (1 - 4m_\ell^2/m_\phi^2)^{3/2}}{8\pi}, \end{aligned} \quad (13)$$

where the function of $\lambda(x, y, z)$ is given by

$$\lambda(x, y, z) = x^2 + y^2 + z^2 - 2xy - 2yz - 2zx. \quad (14)$$

The decay width of the scalar is much smaller than the VLL by an extra small factor θ_L^2 , resulting ϕ to be a potential electrically natural long-lived particle candidate at the detector scale. Its lifetime can be expressed in the limit of $m_\phi \gg m_\ell$ as

$$\tau(\phi) \simeq \left(\frac{3 \times 10^{-9}}{y\theta_L} \right)^2 \left(\frac{50 \text{ GeV}}{m_\phi} \right) \text{ns}. \quad (15)$$

III. EXISTING CONSTRAINTS

The VLL F can decay to leptons. Therefore, it is essential to account for the constraints arising from multi-lepton searches at colliders. Additionally, as the scalar particle couples with leptons, LFV constraints may apply if the Yukawa couplings to different generations of leptons vary. Both of these scenarios contribute to lepton $g - 2$, further constraining these models. In this section, we will thoroughly explore all potential constraints on these two models.

A. Constraints from Heavy Stable Charged Particles Searches

In the first scenario, the F^\pm can be long-lived, while being constrained by the heavy stable charged particles (HSCPs) searches at LHC, using the data collected during 2012 [48] ($\sqrt{s} = 8$ TeV, 18.8 fb^{-1}) and 2016 [49] ($\sqrt{s} = 13$ TeV, 12.9 fb^{-1}) runs. We can translate this constraint into the vector-like lepton with

$$\sigma_{\text{prod}} \times \epsilon(m_F, \theta_L) < \sigma_{\text{LHC}}, \quad (16)$$

where $\epsilon(m_F, \theta_L)$ is the cut efficiency on the specified parameter m_F and θ_L , σ_{LHC} is the cross-section upper limit (95% C.L.) for Modified Drell-Yan Process [48, 49] from LHC searches, and σ_{prod} is the production cross section in our model, also depending on m_F and θ_L . In order to obtain $\epsilon(m_F, \theta_L)$, we adopt the “ tracker+TOF ” approach with the transverse momentum $p_T > 65$ GeV and pseudorapidity $|\eta| < 2.1$ for F^\pm . Furthermore, to ensure that F^\pm traverses the entire detector, we impose the condition that candidate tracks must be measured in the silicon-strip detector and matched to a reconstructed track in the muon system. Specifically, for $|\eta| < 1.2$, the requirement is $r > 7$ m, and for $|\eta| > 1.2$, it is $z > 10$ m [50], where r and z are the transverse and longitudinal decay length of F^\pm respectively. The constraint is shown in Fig. 4 as the shaded gray region, where it takes two parts as these two HSCPs searches focus on different mass regions.

B. Constraints from Multilepton Searches at LHC

For the second scenario, the scalar ϕ can be produced from F^\pm decay and then decay to a pair of lepton. If the ϕ is long-lived enough, it can escape the detector, which acts as missing transverse momentum p_T^{miss} (energy E_T^{miss}). As there are two ϕ produced, there are two possibilities of long-lived particle search. If both ϕ escape the detector, it faces the constraint on the signature of opposite-sign same-flavor (OSSF) leptons pair plus E_T^{miss} from ATLAS [51] and CMS [52]

$$\sigma(pp \rightarrow F^- F^+) \text{Br}(F^\pm \rightarrow \ell^\pm \phi) \cdot \epsilon(\phi^{\text{inv}}) < 0.25 \text{ fb (95\% C.L.)}, \quad (17)$$

where $\epsilon(\phi^{\text{inv}})$ describes the probability of two ϕ s escaping the detector. In our setup, where $y \gg \theta_L$, the branching ratio $\text{Br}(F^\pm \rightarrow \ell^\pm \phi)$ can be approximated as 1. To assess the cut efficiency, we utilized Monte Carlo simulations with MadGraph 5 [53], followed by the application of cuts on p_T , η , $m_{\ell_1 \ell_2}$, m_{T2} , and ΔR following Refs. [51, 52], accounting for the survival efficiency of ϕ to escape the detector. The constraints from this search are represented by gray shaded regions in

Fig. 5 and Fig. 7. It is evident that, for a fixed m_F , the constraints weaken with increasing ϕ mass due to the diminishing production cross-section.

If only one ϕ escapes the detector and the other ϕ decays inside promptly, this scenario faces the constraints from four-lepton searches at ATLAS [54], which set a limit on

$$\sigma(pp \rightarrow F^- F^+, F^\pm \rightarrow \ell^\pm \phi) \cdot \epsilon^{\text{prompt-decay}}(\phi_1) \cdot \epsilon^{\text{inv}}(\phi_2) \lesssim 0.1 \text{ fb (95\%C.L.)}, \quad (18)$$

where $\text{Br}(F^\pm \rightarrow \ell^\pm \phi) = 1$ is applied. Apart from the kinematic cuts efficiency, the efficiency $\epsilon^{\text{prompt-decay}}(\phi_1) \cdot \epsilon^{\text{inv}}(\phi_2)$ also comprises the two geometric requirements, which ensures that one ϕ decays inside while the other escapes the detector, and it can be estimated as

$$\epsilon^{\text{prompt-decay}}(\phi_1) \cdot \epsilon^{\text{inv}}(\phi_2) \equiv \epsilon_{\text{geo}} \simeq \left(1 - e^{-\frac{L_{\text{max}}}{\beta\gamma\tau(\phi)}}\right) e^{-\frac{L_{\text{det}}}{\beta\gamma\tau(\phi)}},$$

where $\beta\gamma$ is Lorentz boosted factor, $L_{\text{max}} \sim \mathcal{O}(\text{mm})$ and $L_{\text{det}} \sim \mathcal{O}(\text{m})$ denote the maximal allowable moving distance for the prompt decay and minimal traveling distance for the escape of ϕ , respectively [12]. By numerical calculation, the maximal $\epsilon_{\text{geo}}^{\text{max}}$ will fall in [0.037%, 0.0037%] when $L_{\text{det}}/L_{\text{max}}$ is in the range [1000, 10000]. With $\sigma(pp \rightarrow F^- F^+) \lesssim 0.07 \text{ pb}$ for $m_F > 200 \text{ GeV}$, this geometrical cut will result in the cross-section much smaller than the experimental limit. Thereby this case is free from the four-lepton searches. The conclusion also applies to the long-lived charged lepton case.

In both scenarios, LLPs have the possibility to decay inside the detector. For the first scenario, the pair produced F^\pm still can decay promptly inside the detector, just need to time the efficiency of

$$\epsilon_{\text{prompt}}^F \simeq \left(1 - e^{-\frac{L_{\text{max}}}{\beta\gamma\tau(F)}}\right)^2.$$

For the second scenario, F^\pm is prompt decay because of ϕ , while ϕ can also decay promptly inside the detector, with efficiency

$$\epsilon_{\text{prompt}}^\phi \simeq \left(1 - e^{-\frac{L_{\text{max}}}{\beta\gamma\tau(\phi)}}\right)^2.$$

Then both two models investigated in this study need to consider the multilepton searches at LHC [11, 12]. The most stringent constraint comes from the inclusive nonresonant multilepton probes of the new singlet prompt decay VLL in Ref. [12], which excluded mass range $m_F \in [125, 150] \text{ GeV}$. In order to translate the constraint, we need to consider the above decay efficiency, which makes the constraint weaker. For our interested mass region $m_F > 200 \text{ GeV}$, our two models are totally safe from this constraint.

C. Constraints from Lepton Flavor Violations

In general, we can have the 3×3 mass matrix for 3 flavor leptons from SM Yukawa interaction. After adding the effective mixing term $\delta \bar{F}_L^0 \ell_R^0 + \text{h.c.}$, we can extend the mass matrix into 4×4 matrix. If we take the case where the second generation lepton μ mixed with F as an example, we have the 4×4 mass matrix as

$$M_{\text{mass}} = \left(\begin{array}{ccc|c} m_{ee} & m_{e\mu} & m_{e\tau} & 0 \\ m_{\mu e} & m_{\mu\mu} & m_{\mu\tau} & 0 \\ m_{\tau e} & m_{\tau\mu} & m_{\tau\tau} & 0 \\ \hline 0 & \delta & 0 & m_F^0 \end{array} \right). \quad (19)$$

For simplicity of parameterization, we can first diagonalize the 3×3 part of the SM mass by two unitary matrices U_L^{SM} and U_R^{SM} , just as Eq. (3), and after the diagonalization the mass matrix can be written as

$$M'_{\text{mass}} = \left(\begin{array}{ccc|c} m'_e & 0 & 0 & 0 \\ 0 & m'_\mu & 0 & 0 \\ 0 & 0 & m'_\tau & 0 \\ \hline \delta \cdot x_1 & \delta \cdot x_2 & \delta \cdot x_3 & m_F^0 \end{array} \right), \quad (20)$$

where the parameters are determined by $x_i = U_{R,i2}^{\text{SM}}$. We can further diagonalize this mass matrix with two unitary matrices U'_L and U'_R . In the leading order of θ_L and θ_R for each element, their explicit forms can be written as

$$U'_L \simeq \left(\begin{array}{ccc|c} 1 - \frac{1}{2}r_{1a}^2\theta_L^2 & x_1x_2r_{12}\theta_R^2 & x_1x_3r_{13}\theta_R^2 & -x_1r_{1a}\theta_L \\ -x_1x_2r_{12}\theta_R^2 & 1 - \frac{1}{2}r_{2a}^2\theta_L^2 & x_2x_3r_{23}\theta_R^2 & -x_2r_{2a}\theta_L \\ -x_1x_3r_{13}\theta_R^2 & -x_2x_3r_{23}\theta_R^2 & 1 - \frac{1}{2}r_{3a}^2\theta_L^2 & -x_3r_{3a}\theta_L \\ \hline x_1r_{1a}\theta_L & x_2r_{2a}\theta_L & x_3r_{3a}\theta_L & 1 - \frac{1}{2}\theta_L^2(r_{1a}^2x_1^2 + r_{2a}^2x_2^2 + r_{3a}^2x_3^2) \end{array} \right), \quad (21)$$

$$U'_R \simeq \left(\begin{array}{ccc|c} 1 - \frac{1}{2}\theta_R^2 & x_1x_2r_{12}\theta_R^2 & x_1x_3r_{13}\theta_R^2 & -x_1\theta_R \\ -x_1x_2\theta_R^2 & 1 - \frac{1}{2}\theta_R^2 & x_2x_3r_{23}\theta_R^2 & -x_2\theta_R \\ -x_1x_3\theta_R^2 & -x_2x_3\theta_R^2 & 1 - \frac{1}{2}\theta_R^2 & -x_3\theta_R \\ \hline x_1\theta_R & x_2\theta_R & x_3\theta_R & 1 - \frac{1}{2}\theta_R^2(x_1^2 + x_2^2 + x_3^2) \end{array} \right),$$

where $r_{ij} \equiv m_{\ell_i}/m_{\ell_j}$, $r_{ia} \equiv m_{\ell_i}/m_{\ell_a}$, ℓ_i refers to e, μ, τ for $i = 1, 2, 3$, respectively, and a denotes the lepton flavor mixed with F , for example $a = 2$ when μ mixed with F . This lepton masses m_{ℓ_a} will receive a correction of order $\mathcal{O}((\delta/m_F)^2)$ as Eq. (7). With these two unitary matrices, in the

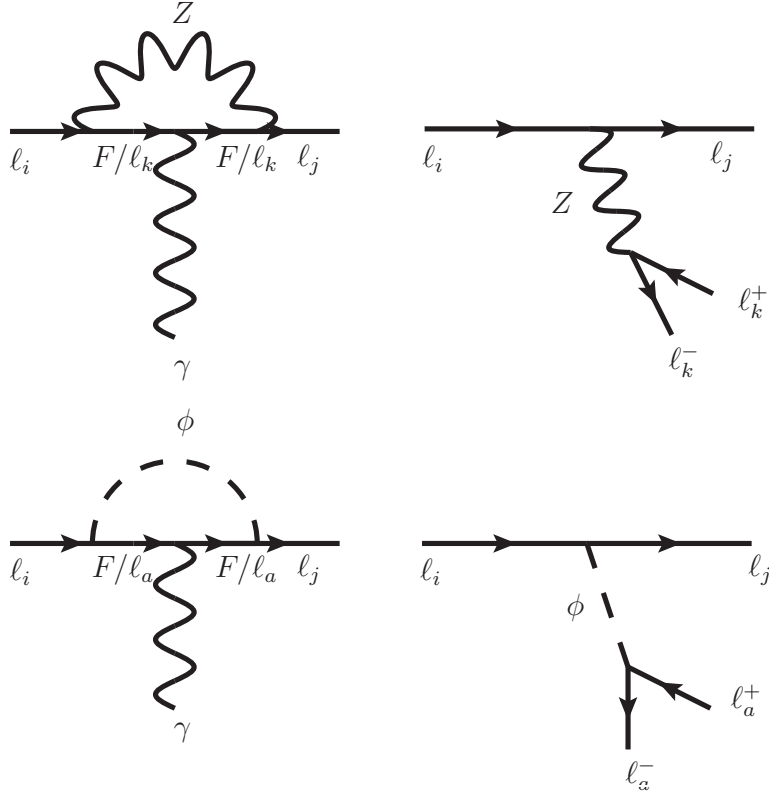


FIG. 1. Feynman diagrams for the lepton flavor violation processes.

following two subsections, we will study the LFVs for the two scenarios introduced in Sec. II A and II B.

1. LFV for VLLS

After the unitary rotations, within the mass eigenstates of SM leptons and VLLs, the interaction parts of Lagrangian for VLLS can be represented as

$$\mathcal{L}_{\text{eff}}^{\text{total}} \supset \mathcal{L}_{\text{eff}}^{\text{FLC}} + \mathcal{L}_{\text{eff}}^{\text{FLV-F}} + \mathcal{L}_{\text{eff}}^{\text{FLV-Z}}, \quad (22)$$

where $\mathcal{L}_{\text{eff}}^{\text{FLC}}$ is the flavor conserving part without ϕ interaction, $\mathcal{L}_{\text{eff}}^{\text{FLV-F}}$ represents the flavor violating interaction terms between F and SM leptons, contributing to the decays of F and leptons $g-2$, $\mathcal{L}_{\text{eff}}^{\text{FLV-Z}}$ stands for the flavor violating terms of SM leptons related to Z boson. To the leading

order, the flavor-conserving part mediated by SM bosons can be reduced to

$$\begin{aligned} \mathcal{L}_{\text{eff}}^{\text{FLC}} = & \bar{F}(i\partial_\mu - eA_\mu + e \tan \theta_W Z_\mu)\gamma^\mu F - m_F \bar{F}F + \sum_{i=1,2,3} \bar{\ell}_i(i\partial_\mu - eA_\mu + e \tan \theta_W Z_\mu)\gamma^\mu \ell_i - m_{\ell_i} \bar{\ell}_i \ell_i \\ & + \sum_{i=1,2,3} \frac{1}{2} \frac{e}{\sin \theta_W \cos \theta_W} Z_\mu \bar{\ell}_{iL} \gamma^\mu \ell_{iL} - \frac{e}{\sqrt{2} \sin \theta_W} (W_\mu^+ \bar{\nu}_{iL} \gamma^\mu \ell_{iL} + \text{h.c.}), \end{aligned} \quad (23)$$

and the flavor-violating parts mediated by SM bosons can be formulated as

$$\begin{aligned} \mathcal{L}_{\text{eff}}^{\text{FLV-F}} \simeq & \sum_{i=1,2,3} \left(-\frac{1}{2} \frac{e}{\sin \theta_W \cos \theta_W} U'_{L,44} U'_{L,i4} Z_\mu \bar{F}_L \gamma^\mu \ell_{iL} - \frac{e}{\sqrt{2} \sin \theta_W} U'_{L,4i} W_\mu^+ \bar{\nu}_{iL} \gamma^\mu F_L + \text{h.c.} \right) \\ \simeq & \frac{e}{\sin \theta_W} \sum_{i=1,2,3} x_i r_{ia} \theta_L \left(\frac{1}{2} \frac{1}{\cos \theta_W} Z_\mu \bar{F}_L \gamma^\mu \ell_{iL} - \frac{1}{\sqrt{2}} W_\mu^+ \bar{\nu}_{iL} \gamma^\mu F_L + \text{h.c.} \right), \\ \mathcal{L}_{\text{eff}}^{\text{FLV-Z}} \simeq & - \sum_{i,j=1,2,3,(i \neq j)} \left(\frac{1}{2} \frac{e}{\sin \theta_W \cos \theta_W} U'_{L,i4} U'_{L,j4} Z_\mu \bar{\ell}_{iL} \gamma^\mu \ell_{jL} \right) \\ \simeq & - \frac{1}{2} \frac{e}{\sin \theta_W \cos \theta_W} \sum_{i,j=1,2,3,(i \neq j)} x_i x_j r_{ia} r_{ja} \theta_L^2 Z_\mu \bar{\ell}_{iL} \gamma^\mu \ell_{jL}. \end{aligned} \quad (24)$$

For the electromagnetic current interaction, due to the uniform interaction among different generations, there is no electromagnetic flavor violation term. Thus the dominant origin of LFV comes from the weak interaction, where the left-hand interaction has different forms to the right one. For this model, among the LFV processes related to muons, taus, and bosons (Z , h) [55], the current strongest experimental upper limits come from the branching ratio measurement of $\mu \rightarrow eee$, $\tau \rightarrow \ell_i \ell_j \ell_j$ and $\ell_i \rightarrow \ell_j \gamma$, which respectively require [55–59]

$$\text{Br}(\mu \rightarrow eee) < 10^{-12}, \quad \text{Br}(\tau \rightarrow \ell_i \ell_j \ell_j) \lesssim 2.7 \times 10^{-8}, \quad \text{Br}(\ell_i \rightarrow \ell_j \gamma) \lesssim 4.2 \times 10^{-13}, \quad (25)$$

where among all the FLV processes, the strongest ones for $\text{Br}(\tau \rightarrow \ell_i \ell_j \ell_j)$ and $\text{Br}(\ell_i \rightarrow \ell_j \gamma)$ are adopted as the upper limits (concretely, they are from the measurements of $\tau \rightarrow e\mu\mu/eee \lesssim 2.7 \times 10^{-8}$ and $\mu^+ \rightarrow e^+\gamma \lesssim 4.2 \times 10^{-13}$). In the upper panels of Fig. 1, the Feynman diagrams for these LFV processes are plotted. The corresponding branching ratios can be estimated as

$$\begin{aligned} \text{Br}(\ell_i \rightarrow \ell_j \ell_k \ell_k) & \sim (x_i x_j r_{ia} r_{ja} \theta_L^2)^2 \\ & \sim 10^{-10} \left(\frac{x_i}{1}\right)^2 \left(\frac{x_j}{1}\right)^2 \left(\frac{r_{ia}}{10^{-3}}\right)^2 \left(\frac{r_{ja}}{1}\right)^2 \left(\frac{\theta_L}{10^{-1}}\right)^4, \\ \text{Br}(\ell_i \rightarrow \ell_j \gamma) & \sim (x_i x_j r_{ia} r_{ja} \theta_L^2)^2 \cdot \frac{400\pi^4 \alpha_{\text{EM}}}{3G_F^2 m_Z^4} \\ & \sim 1.7 \times 10^{-14} \left(\frac{x_i}{1}\right)^2 \left(\frac{x_j}{1}\right)^2 \left(\frac{r_{ia}}{10^{-3}}\right)^2 \left(\frac{r_{ja}}{1}\right)^2 \left(\frac{\theta_L}{10^{-2}}\right)^4. \end{aligned} \quad (26)$$

These constraints can be easily satisfied for the muon case ($a = 2$), as long as we require $\theta_L < 10^{-2}$ with general $x_i \sim \mathcal{O}(1)$.

2. LFV for VLLWS

There is the additional ϕ -Yukawa interaction, $\mathcal{L}_{\text{eff}}^\phi$ in the VLLWS case, which needs to be recalculated. For this interaction, if the SM lepton in $y\phi\bar{F}_L^0\ell_R^0 + \text{h.c.}$ term is the initial flavor eigenstate, then with the unitary rotations of SM parts by $U_{L/R}^{\text{SM}}$, this interaction will be transformed to

$$\begin{aligned}\mathcal{L}_{\text{eff}}^\phi &= y\phi(\bar{e}_L^0, \bar{\mu}_L^0, \bar{\tau}_L^0, \bar{F}_L^0) \left(\begin{array}{ccc|c} 0 & 0 & 0 & 0 \\ 0 & 0 & 0 & 0 \\ 0 & 0 & 0 & 0 \\ \hline 0 & 1 & 0 & 0 \end{array} \right) \begin{pmatrix} e_R^0 \\ \mu_R^0 \\ \tau_R^0 \\ F_R^0 \end{pmatrix} + \text{h.c.} \\ &= y\phi(\bar{e}'_L, \bar{\mu}'_L, \bar{\tau}'_L, \bar{F}'_L) \left(\begin{array}{ccc|c} 0 & 0 & 0 & 0 \\ 0 & 0 & 0 & 0 \\ 0 & 0 & 0 & 0 \\ \hline x_1 & x_2 & x_3 & 0 \end{array} \right) \begin{pmatrix} e'_R \\ \mu'_R \\ \tau'_R \\ F'_R \end{pmatrix} + \text{h.c.}\end{aligned}\quad (27)$$

After the further diagonalization of the mass matrix M'_{mass} via the unitary matrices U'_L and U'_R , to the leading order, this interaction in the mass eigenstates will be finally simplified to

$$\mathcal{L}_{eff}^\phi \simeq y\phi(\bar{e}_L, \bar{\mu}_L, \bar{\tau}_L, \bar{F}_L) \left(\begin{array}{ccc|c} -r_{1a}x_1^2\theta_L & -r_{1a}x_1x_2\theta_L & -r_{1a}x_1x_3\theta_L & 0 \\ -r_{2a}x_1x_2\theta_L & -r_{2a}x_2^2\theta_L & -r_{2a}x_2x_3\theta_L & 0 \\ -r_{3a}x_1x_3\theta_L & -r_{3a}x_2x_3\theta_L & -r_{3a}x_3^2\theta_L & 0 \\ \hline x_1 - \frac{x_1^3\theta_R^2}{2} & x_2 - \frac{x_2^3\theta_R^2}{2} & x_3 - \frac{x_3^3\theta_R^2}{2} & \theta_R(x_1^2 + x_2^2 + x_3^2) \end{array} \right) \begin{pmatrix} e_R \\ \mu_R \\ \tau_R \\ F_R \end{pmatrix} + \text{h.c.}\quad (28)$$

The last row will directly introduce order $\mathcal{O}(x_i)$ interactions between different SM lepton flavors and VLLs, mediated by scalar ϕ , which results in sizeable contributions to the LFV processes. Especially, for $\ell_i \rightarrow \ell_j\gamma$, the branching fraction with the Feynman diagram shown in the left-lower panel of Fig. 1 can be derived as

$$\text{Br}(\ell_i \rightarrow \ell_j\gamma) \simeq \frac{\pi^3 \alpha_{\text{EM}} (y^2 x_i x_j)^2 \left(m_F^6 - 6m_F^4 m_\phi^2 + 3m_F^2 m_\phi^4 + 2m_\phi^6 + 12m_F^2 m_\phi^4 \ln\left(\frac{m_F}{m_\phi}\right) \right)^2}{3G_F^2 (m_F^2 - m_\phi^2)^8}, \quad (29)$$

which is derived under the condition $m_e \rightarrow 0$, $m_F > m_\phi \gg m_\mu$. The measurement of $\mu \rightarrow e\gamma$ [56] places strong limits on our parameters, which requires

$$y < 6.8 \times 10^{-4} \left(\frac{1}{x_1}\right)^{1/2} \left(\frac{1}{x_2}\right)^{1/2} \left(\frac{m_F}{200 \text{ GeV}}\right).$$

This strong constraint can be easily avoided in several cases. On the one hand, one can take the ϕ -interaction to be under the mass eigenstate of SM leptons just as the usual considerations in $U(1)_{L_\mu-L_\tau}$ (the SM leptons are taken to be the mass eigenstates in the $U(1)_{L_\mu-L_\tau}$) [60], which can directly prevent the mixing between different generations as Eq. (27). On the other hand, these LFVs can be well avoided or solved theoretically. The relevant terms related to LFVs come from the off-diagonal mixing between SM leptons, and this can be forbidden by introducing a global symmetry just as Ref. [47], which is exactly the case we discussed in Sec. II, and it can directly prevent the mixing between different SM lepton generations.

In our study, we follow the first case that the ϕ -interaction is in the SM mass eigenstates, to avoid the strong LFV constraints. Then, the Lagrangian after $U'_{L/R}$ rotations can be represented as

$$\begin{aligned}
\mathcal{L}_{\text{eff}}^\phi &= y\phi \left(\sum_{i,j=1,2,3} \left(U'_{L,i4} U'_{R,ja} \bar{\ell}_{iL} \ell_{jR} + \text{h.c.} \right) + \sum_{j=1,2,3} \left(U'_{L,44} U'_{R,ja} \bar{F}_L \ell_{jR} + U'_{L,j4} U'_{R,4a} \bar{\ell}_{jL} F_R + \text{h.c.} \right) \right) \\
&\quad + y\phi \left(U'_{L,44} U'_{R,4a} \bar{F}_L F_R + \text{h.c.} \right), \\
&\simeq y\phi \left(x_a \theta_R \bar{F} F + (\bar{F}_L \ell_{aR} - x_a^2 \theta_L \theta_R \bar{\ell}_{aL} F_R + \text{h.c.}) + \sum_{i=1,2,3} \left(-x_i r_{ia} \theta_L (\bar{\ell}_{iL} \ell_{aR} + \text{h.c.}) \right) \right. \\
&\quad \left. + \sum_{i=1,2,3(i \neq a)} \left(\mathcal{O}(x_i x_a r_{ia}) \cdot \theta_R^2 \bar{F}_L \ell_{iR} - x_i x_a r_{ia} \theta_L \theta_R \bar{\ell}_{iL} F_R + \text{h.c.} \right) + \mathcal{O}(\theta_{L/R}^3) \right).
\end{aligned} \tag{30}$$

In Fig. 1, the LFV Feynman diagrams for this model are plotted, where the lower part refers to the contributions from ϕ -interaction. The leading contributions to the LFV processes arise mainly from the ϕ -term, which is

$$\begin{aligned}
\text{Br}(\ell_a \rightarrow \ell_i \gamma) &\simeq \frac{\pi^3 \alpha_{\text{EM}} (x_i x_a r_{ia} y^2 \theta_R^2)^2 \left(m_F^6 - 6m_F^4 m_\phi^2 + 3m_F^2 m_\phi^4 + 2m_F^6 + 12m_F^2 m_\phi^4 \ln\left(\frac{m_F}{m_\phi}\right) \right)^2}{3G_F^2 (m_F^2 - m_\phi^2)^8} \\
&\simeq 3.5 \times 10^{-15} \left(\frac{x_i}{1}\right)^2 \left(\frac{x_a}{1}\right)^2 \left(\frac{r_{ia}}{10^{-3}}\right)^2 \left(\frac{y\theta_R}{10^{-2}}\right)^4 \left(\frac{200 \text{ GeV}}{m_F}\right)^4.
\end{aligned} \tag{31}$$

If we choose the parameter space as

$$\left\{ x_i, x_a < 1, r_{ia} < 10^{-3}, y\theta_R < 10^{-2}, m_F > 200 \text{ GeV} \right\}, \tag{32}$$

there is no pressure from the LFV two-body decay $\ell_a \rightarrow \ell_i \gamma$ constraints.

Next, we will consider the 3-body decay process $\ell_i \rightarrow \ell_j \ell_k \ell_k$. We choose the muon-specific VLL case ($a = 2$) as an example. The only kinematical allowed muon decay process is $\mu \rightarrow eee$. This LFV process can be realized by ϕ mediator, which is heavily suppressed by a combined factor

of $(y^2\theta_L^2\theta_R^2x_1x_2r_{12})^2 / (G_F^2m_\phi^4)$. Thus, we only need to consider the channel mediated by Z boson dominates, which is already discussed in Eq. (26). The other relevant 3-body LFV decay process is $\tau \rightarrow \mu\mu\mu$, which decay branching ratio can be estimated by

$$\begin{aligned} \text{Br}(\tau \rightarrow \mu\mu\mu) &\sim \theta_L^4 + \frac{\sqrt{2}(y^2x_2x_3r_{32})\theta_L^4}{16G_Fm_\phi^2} + \frac{(y\theta_L)^4(x_2x_3r_{32})^2}{128G_F^2m_\phi^4} \\ &\sim 10^{-8} \left[\left(\frac{\theta_L}{10^{-2}}\right)^4 + 0.8 \left(\frac{\theta_L}{10^{-2}}\right)^2 \left(\frac{x_2}{1}\right) \left(\frac{x_3}{1}\right) \left(\frac{y\theta_L}{5 \times 10^{-4}}\right)^2 \left(\frac{20 \text{ GeV}}{m_\phi}\right)^2 \right. \\ &\quad \left. + 0.7 \left(\frac{x_2}{1}\right)^2 \left(\frac{x_3}{1}\right)^2 \left(\frac{y\theta_L}{0.5 \times 10^{-3}}\right)^4 \left(\frac{20 \text{ GeV}}{m_\phi}\right)^4 \right]. \end{aligned} \quad (33)$$

Considering the stringent experimental constraints with $\text{Br}(\tau \rightarrow \mu\mu\mu) < 2.1 \times 10^{-8}$ [59], it is evident that our models are safe for this constraint, if $y\theta_L < 0.5 \times 10^{-3}$. Therefore, combining all the LFV processes, the experimental constraints can be easily satisfied, as long as we require

$$\{\theta_L < 10^{-2}, y\theta_R < 10^{-2}, y\theta_L < 0.5 \times 10^{-3}, m_F > 200 \text{ GeV and } m_\phi > 20 \text{ GeV}\}. \quad (34)$$

In addition, these conditions are consistent with the parameter regions of interest in our LLP study.

In this subsection, we have discussed lepton flavor violation in the context of the VLLWS model, which includes an additional scalar field. If the Yukawa coupling $y\phi\bar{F}_L^0\ell_R^0$ involves the flavor eigenstates of the lepton, it becomes subject to strong constraints from LFV decays, such as $\mu \rightarrow e\gamma$. As a result, we are led to assume that ℓ must either be a SM mass eigenstate or be associated with a global symmetry that confines the coupling of ϕ to a single mass eigenstate. Subsequently, when considering this model, we adopt the assumption that ℓ is indeed a SM mass eigenstate. With this assumption in place, we can express the LFV constraints concisely through Eq. (34), which is relatively easy to meet these constraints.

D. Constraints from $g - 2$

The interactions as shown in the previous subsection will directly contribute to the muon and electron $g - 2$. We will consider the constraints from experiments [61–64]

$$\begin{aligned} (g - 2)_\mu^{\text{BSM}} &< 2.49 \times 10^{-9}, \\ (g - 2)_e^{\text{BSM}} &< 9.8 \times 10^{-13}. \end{aligned} \quad (35)$$

In Fig. 2, the Feynman diagrams for the loop processes illustrate the ϕ and Z mediated contributions in the context of BSM physics. The crucial chiral flip is limited to occurring along the

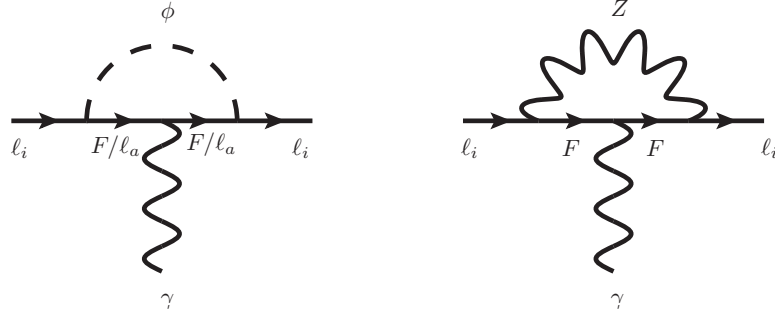


FIG. 2. The Feynman diagrams for the loop processes mediated by ϕ and Z in the context of BSM physics.

internal and external ℓ lines; it cannot affect the vector-like fermion F . This is due to the fact that ϕ predominantly couples to $\bar{F}_L \ell_R$, while its coupling to $\bar{\ell}_L F_R$ is heavily suppressed, as indicated by the small parameter combination $\theta_L \theta_R$ in Eq. (30). Similarly, for the Z mediated diagram, it holds true that the chiral flip does not happen in the F line, as its off-diagonal flavor coupling to F - ℓ only occurs for the left-handed fermions in Eq. (24). The corresponding contributions for the diagrams can be derived as

$$\begin{aligned}
 (g-2)_{\ell_i}^{F,\phi} &\simeq \begin{cases} \frac{y^2 m_{\ell_i}^2 (m_F^6 - 6m_F^4 m_\phi^2 + 3m_F^2 m_\phi^4 + 2m_\phi^6 + 12m_F^2 m_\phi^4 \ln(\frac{m_F}{m_\phi}))}{96\pi^2 (m_F^2 - m_\phi^2)^4} + \mathcal{O}\left(\frac{m_{\ell_i}}{m_F}\right)^4 & (m_F > m_\phi \gg m_{\ell_i}), \\ \frac{y^2 m_{\ell_i}^2}{192\pi^2 m_F^2} + \mathcal{O}\left(\frac{m_{\ell_i}}{m_F}\right)^4 & (m_\phi = m_F \gg m_{\ell_i}), \end{cases} \\
 (g-2)_{\ell_i}^{\ell_a,\phi} &= \frac{(yx_i r_{ia} \theta_L)^2 m_{\ell_i}^2}{48\pi^2 m_\phi^2} + \mathcal{O}\left(\frac{m_{\ell_i}}{m_\phi}\right)^4, \\
 (g-2)_{\ell_i}^{F,Z} &= -\left(\frac{1}{2} \frac{e}{\sin \theta_W \cos \theta_W} yx_i r_{ia} \theta_L\right)^2 \cdot \left(\frac{5m_{\ell_i}^2}{96\pi^2 m_Z^2} + \frac{m_{\ell_i}^2}{16\pi^2 m_F^2} + \frac{m_{\ell_i}^4}{192\pi^2 m_Z^2 m_F^2}\right) + \mathcal{O}\left(\frac{m_{\ell_i}^2 m_Z^2}{m_F^4}\right). \tag{36}
 \end{aligned}$$

The contribution in the first line, originating from F and ϕ , is proportional to y^2 and is the dominant component. While the last two contributions are proportional to $(yx_i r_{ia} \theta_L)^2$, which is significantly smaller than the first one, as per our specified parameter configuration,

$$\{\theta_L < 10^{-2}, m_F > 200 \text{ GeV and } m_\phi > 20 \text{ GeV}\}. \tag{37}$$

Hence, we predominantly focus on the first contribution when estimating the impact of the lepton

$g - 2$ constraint, which leads to

$$(g - 2)_{\ell_i}^{F,\phi} \simeq \begin{cases} 2.64 \times 10^{-10} \left(\frac{y}{1}\right)^2 \left(\frac{m_{\ell_i}}{0.1 \text{ GeV}}\right)^2 \left(\frac{200 \text{ GeV}}{m_F}\right)^2 & (m_F > m_\phi \gg m_{\ell_i}), \\ 1.32 \times 10^{-10} \left(\frac{y}{1}\right)^2 \left(\frac{m_{\ell_i}}{0.1 \text{ GeV}}\right)^2 \left(\frac{200 \text{ GeV}}{m_F}\right)^2 & (m_\phi = m_F \gg m_{\ell_i}), \end{cases} \quad (38)$$

where we can typically set $y = 1$ to ensure compliance with this constraint for the parameter spaces of interest to us.

To summarize the findings in Section III, our study primarily places constraints on the properties of long-lived charged leptons and long-lived scalars. These constraints mainly stem from searches for Heavy Stable Charged Particles and the investigation of events at the LHC featuring Opposite-Sign-Same-Flavor dileptons and missing transverse momentum. In contrast, the effects of Lepton Flavor Violation measurements and the lepton anomalous magnetic moment are negligible in the specific parameter regions that have been the focus of our investigation. For the sake of simplicity and clarity in our analysis of Long-Lived Particle signatures, we will concentrate on our chosen scenario and parameter space, and consequently, we will not consider the small LFV couplings in off-diagonal elements.

IV. LONG-LIVED PARTICLE SIGNATURES AT COLLIDERS

Following the two scenarios discussed above, we will talk about the two kinds of long-lived signatures, one treats vector-like lepton F^\pm as the long-lived particle, while the other treats the scalar particle ϕ as the long-lived particle. For both models, the VLL F^\pm can be pairs produced via Drell-Yan processes at the LHC. In this section, we will explore the long-lived particle signals at the future HL-LHC (CEPC), with center-of-mass energy $\sqrt{s} = 13 \text{ TeV}$ (240 GeV) and the integrated luminosity $\mathcal{L} = 3 \text{ ab}^{-1}$ (5.6 ab^{-1}), which satisfied the constraints considered in Sec. III. We only consider the case where VLLs are coupled with second-generation leptons at HL-LHC to reduce the background, because due to higher misidentification of electrons, usually, electrons have higher backgrounds than muons [65, 66]. While for the searches at CEPC, we assume that VLL and its accompanying scalar only mix with the first-generation lepton.

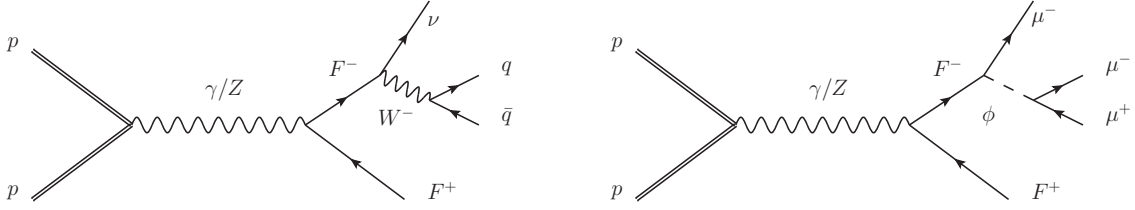


FIG. 3. Feynman diagram for the production and decay of long-lived vector-like lepton and scalar at LHC. An example diagram for the signal process is shown in the left panel, and long-lived F results in kink tracks signal at LHC. While in the right panel, long-lived scalar ϕ leads to a displaced vertex or time delay signal at LHC.

A. Long-lived vector-like lepton

In the first case, the vector-like lepton F^\pm could be pair produced ($pp \rightarrow F^- F^+$) via a pure electroweak process. Then F^\pm could decay into two distinct channels: $F^\pm \rightarrow W^\pm \nu$ or $Z\mu^\pm$, with similar branching ratios, both widths are suppressed by the mixing angle θ_L . Remarkably, all observable F^\pm decay channels exhibit a comparable level of sensitivity within the parameter space of m_F and θ_L . Consequently, we choose one decay chain as a representative example. We employ an inclusive search strategy that at least one of the F^\pm decays inside the detector. The complete signal process can be expressed as follows:

$$pp \rightarrow F^- F^+, F^- \rightarrow W^- \nu_\mu, W^- \rightarrow q\bar{q}. \quad (39)$$

The corresponding Feynman diagram illustrating the production and decay of this specific process is depicted in the left panel of Fig. 3.

In order to search long-lived VLL F^\pm , we can effectively employ search strategies centered around kink track (KT) signatures at the HL-LHC. These strategies necessitate the reconstruction of both the charged mother and daughter particles within the tracker. To accomplish this, we must apply specific selection criteria. These distinct kink tracks can be readily identified within the Transition Radiation Tracker (TRT) component of the ATLAS detector, as described in [67]. The selection conditions, following [67], are:

$$\begin{aligned} \text{KT} : \quad & p_T^F > 100 \text{ GeV}, |\eta_F| < 0.63, 0.1 < \Delta\phi < \pi/2, \\ & 563 \text{ mm} < r_F < 863 \text{ mm}, |z_F| < 712 \text{ mm}, \\ & p_T^q > 10 \text{ GeV}, |z_F/r_F| > |p_z^\mu/p_T^\mu|, \end{aligned} \quad (40)$$

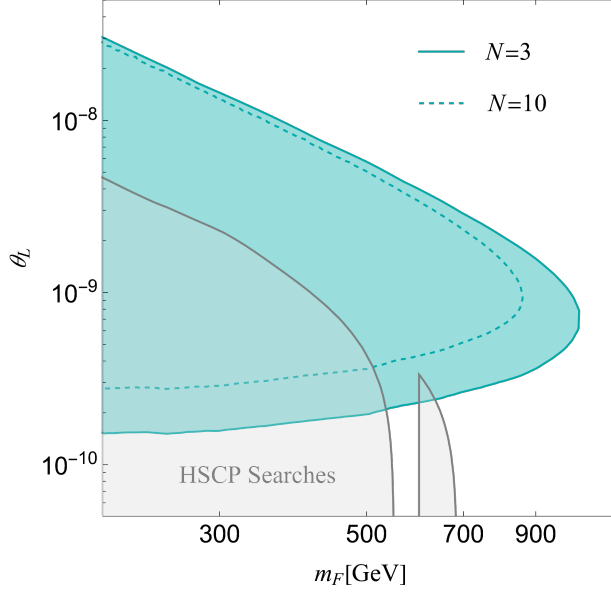


FIG. 4. The expected sensitivity at HL-LHC as the function of vector-like lepton mass m_F , with $\mathcal{L} = 3 \text{ ab}^{-1}$ and $\sqrt{s} = 13 \text{ TeV}$. The cyan shaded region represents signal event number $N_{\text{sig}} = 3$, while the dashed cyan line represents $N_{\text{sig}} = 10$. The gray-shaded region is the constraint from HSCPs searches of CMS [48, 49], where it takes two parts as these two HSCPs searches focus on different mass regions.

where p_T^F and p_T^q represent the transverse momentum of the parent particle F^- and the daughter particle q (or \bar{q}), respectively. η_F is pseudorapidity of F^- , which cut is chosen to ensure a reasonable probability for F^- to traverse the full TRT volume before decaying. $\Delta\phi$ is the kink angle (representing the relative azimuthal angle between F^- and its decay products, q or \bar{q}), which is deliberately set to a substantial value to effectively suppress background events. Additionally, r_F and $|z_F|$ correspond to the transverse and longitudinal decay length of F^- , defined as the distance from the beam axis and along the beam axis from the nominal collision point, respectively. The cut on r_F and z_F ensures that the charged parent particle F^- decays within the TRT volume but prior to the 3rd module, while the decay product can traverse the outermost layer of the barrel TRT. Importantly, the described selection rule necessitates the identification of at least one kink track.

It is noteworthy that while hadronic backgrounds stemming from the SM, such as in-flight decays of π^\pm or K^\pm , and stable charged hadrons undergoing hadronic interactions with trackers may modify their direction, these potential background sources can be significantly mitigated by the application of the aforementioned selection criteria [67].

The quantity of signal events meeting these selection criteria can be determined using the following expression:

$$N_{\text{sig}} = \mathcal{L} \cdot \sigma_{\text{prod}} \cdot \epsilon_{\text{cut}}, \quad (41)$$

where $\mathcal{L} = 3 \text{ ab}^{-1}$ represents the integrated luminosity, σ_{prod} stands for the production cross-section for $pp \rightarrow F^+F^-$, and ϵ_{cut} accounts for the cumulative cut efficiency. We ascertain the detection efficiency for the long-lived vector-like lepton with kink tracks at HL-LHC by the simulations with the MadGraph 5. Based on the simulated cut efficiency, the expected sensitivity at HL-LHC is depicted in Fig. 4. The cyan contour region outlines the regions where the signal event $N_{\text{sig}} > 3$, corresponding to a 95% (C.L.), while the dashed cyan line signifies $N_{\text{sig}} = 10$. The results illustrate that utilizing the kink track signatures can probe the parameter space for $\theta_L \in [10^{-10}, 10^{-7}]$ within the mass range of VLL $m_F \in [200, 950] \text{ GeV}$.

B. Long-lived scalar particle

In the second case, the pair produced VLL F^\pm promptly decays to $\phi\ell^\pm$. The scalar ϕ could be a long-lived particle, which acts as a displaced vertex (decay to a pair of leptons $\phi \rightarrow \ell^+\ell^-$) or flying outside of the detector. The full signal process is

$$pp \rightarrow F^-F^+, F^\pm \rightarrow \phi\ell^\pm, \phi \rightarrow \ell^+\ell^-, \quad (42)$$

and the corresponding Feynman diagram is shown in the right panel of Fig. 3. We consider the inclusive search, where at least one long-lived ϕ decays into an OSSF lepton pair inside the detector. To achieve the LLPs requirement, the lifetime and dynamical properties of ϕ are crucial, which depend on the m_ϕ , m_F , and θ_L . Especially, the dynamic property of ϕ and its decay products $\ell^+\ell^-$ is determined by the relationship between m_F and m_ϕ , where ℓ chosen as μ in this case. In this work, after assuming $y = 1$, three simplified benchmarks on the free physical parameters $\{m_F, m_\phi, \theta_L\}$ are considered, which are

1. $\{m_F/m_\phi = 2, 5, 10, m_F > 200 \text{ GeV}, \theta_L \ll 1\}$,
2. $\{m_\phi \in [20 \text{ GeV}, m_F], m_F = 1 \text{ TeV}, 1.2 \text{ TeV}, \theta_L \ll 1\}$,
3. $\{m_\phi = 100 \text{ GeV}, 300 \text{ GeV}, 500 \text{ GeV}, m_F > 200 \text{ GeV}, \theta_L \ll 1\}$.

Numerous strategies have been proposed to search for long-lived particles at the LHC [68]. These strategies employ distinct signatures associated with LLPs, including Displaced Vertices (DV)

and Time Delays (TD), which offer effective means to reduce Standard Model (SM) backgrounds significantly. In this study, we will implement two methods characterized by these aforementioned signatures.

For both methods, it is imperative to leverage the OSSF leptons from the prompt decay of F^\pm . These VLLs rapidly undergo decay, resulting in a pair of high-energy and promptly detectable OSSF leptons. Such OSSF leptons can effectively serve as temporal markers for the primary vertex, triggering the identification of signal events. The concept of employing a hard lepton trigger has been explored in numerous experimental contexts. For instance, in the context of the CMS Phase-2 upgrade of the Level-1 trigger [69], the trigger thresholds (incorporating a track trigger) stipulate $p_T > 27$ (31) GeV for isolated (non-isolated) electrons and 18 GeV for muons. These thresholds can be further relaxed for pairs of same-flavor leptons. As an example, within the trigger menu of ATLAS Run-2 [70], the requirements are $p_T > 15$ GeV (18 GeV) for each muon (electron), or $p_T^{\mu_1} > 23$ GeV and $p_T^{\mu_2} > 9$ GeV.

Given our primary focus on heavy vector-like leptons, whose prompt decay inherently results in two high-energy leptons, the stringent trigger threshold of $p_T^{\mu,F} > 30$ GeV is adopted in our simulations to further suppress SM backgrounds. Therefore, it is important to note that this trigger configuration is notably conservative in its approach.

1. *Displaced vertex search*

As discussed previously the high p_T cuts on the OSSF muons pair from the vector-like F^\pm decay can not only work as the trigger but also attenuate the SM backgrounds. In addition, we take into account the DV characteristics of the long-lived ϕ particle, which encompasses properties related to the decay position concerning the primary vertex and the muon-jet (DMJ). Our selection criteria align with the specific cuts outlined in [71]:

$$\text{DMJ} : p_T^{\mu,F} > 30 \text{ GeV}, p_T^{\mu,\phi} > 5 \text{ GeV}, r_\phi < 30 \text{ cm}, d_0^{\mu,\phi} > 1 \text{ mm}, \quad (44)$$

where $p_T^{\mu,F/\phi}$ denotes the transverse momentum of muons arising from the decays of F/ϕ , respectively. Furthermore, r_ϕ represents the radial displacement of the ϕ particle, while $d_0^{\mu,\phi}$ corresponds to the transverse impact parameter. It is worth noting that applying the above cuts has been shown to effectively reduce background contributions to a negligible level, following [72].

2. Time delay search

Time information can be effectively captured with the introduction of dedicated timing layers in future upgrades of the HL-LHC, as exemplified by CMS implementing the Minimum Ionizing Particle (MIP) timing detector [73, 74], ATLAS incorporating the High Granularity Timing Detector [75], and other experiments adopting similar timing layers, including LHCb [76], MATHUSLA [77, 78], FASER [79, 80], and CODEX-b [81]. This invaluable timing information serves multiple purposes, as it not only addresses challenges related to pile-up events and enhances the precision of particle measurements, but also distinguishes new long-lived signals from SM backgrounds.

Typically, SM particles travel at nearly the speed of light, while LLPs, such as ϕ , move at much slower velocities and exhibit a noticeable time delay in their decay. The time delay can be defined as [82]

$$\Delta t_\ell = L_\phi/\beta_\phi + L_\ell/\beta_\ell - L_{\text{SM}}/\beta_{\text{SM}} \quad (45)$$

for this process ($\phi \rightarrow \ell\bar{\ell}$), where β and L denote the velocity and the moving distance, and SM denotes a trajectory from the interaction point to the arrival point at the detector by SM particle. For convenience, the trajectories of ϕ and decay products are assumed to be straight, and $\beta_l \simeq \beta_{\text{SM}} \simeq 1$.

Therefore, we also consider the TD signatures of heavy LLPs on CMS, and the cuts are chosen as follows [71, 83]

$$\text{TD} : p_T^{\mu,F} > 30 \text{ GeV}, p_T^{\mu,\phi} > 5 \text{ GeV}, |\eta| < 2.4, \Delta t_{\mu,\phi} > 0.3 \text{ ns}, 5 \text{ cm} < r_\phi < 1.17 \text{ m}, z_\phi < 3.04 \text{ m}, \quad (46)$$

where η denotes the muons pseudo-rapidity (as we choose μ for SM lepton). The cuts on the radial displacements r_ϕ , longitudinal displacements z_ϕ and the TD $\Delta t_{\mu,\phi}$ ensure the decay vertex is within the CMS MIP timing detector and reduce the SM backgrounds. The simultaneous presence of promptly produced OSSF muon pairs, combined with the availability of timing information, plays a crucial role in significantly suppressing SM backgrounds, as evidenced in [82]. Consequently, in this study, we conservatively treat SM backgrounds as negligible. It is worth noting that several other established and proposed LHC experiments, including MATHUSLA, FASER, and CODEX-b, hold the potential to explore the long-lived signature associated with the scalar ϕ . However, these experiments share similar features regarding constraints on the OSSF lepton pair and missing transverse momentum, as outlined in Section III. Consequently, we do not delve into their details within this discussion.

Based on the two search methods, the signal event number of these LLPs can be written as

$$N_{\text{sig}}^{\phi} = \mathcal{L} \cdot \sigma(pp \rightarrow F^- F^+) \cdot P^{\text{LLP}}(\phi) \cdot \epsilon_{\text{cut}}, \quad (47)$$

where $P^{\text{LLP}}(\phi)$ stands for the probability of ϕ decaying within the designated detector volume, and ϵ_{cut} represents the total cut efficiency. To assess the signal efficiency, we conducted corresponding Monte Carlo (MC) simulations of events at the parton level using MadGraph 5. The determination of $P^{\text{LLP}}(\phi)$ for a given lifetime relies on the kinematics of ϕ and μ .

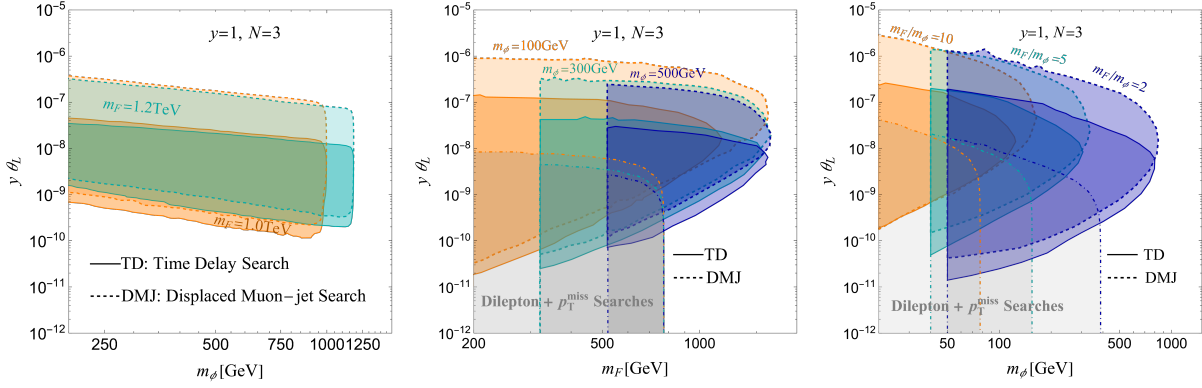


FIG. 5. The expected 95% C.L. sensitivities at HL-LHC for the long-lived scalar case as a function of the scalar or vector-like lepton mass m_ϕ or m_F for $\mathcal{L} = 3 \text{ ab}^{-1}$ and $\sqrt{s} = 13 \text{ TeV}$. From left to right, the m_F fixed, m_ϕ fixed, and three mass ratios m_F/m_ϕ fixed cases are shown, respectively. Besides, the constraints from LHC dilepton and missing energy or transverse momentum searches are also shown with gray-shaded regions with the corresponding colors as boundaries for every case.

Finally, the sensitivities in the $y\theta_L - m_F(m_\phi)$ plane at HL-LHC are presented in Fig. 5 for three distinct benchmarks (Eq. (43)). In this context, the threshold for the number of required signal events is set as $N \geq 3$, which precisely corresponds to the exclusion limit at a 95% C.L. with zero backgrounds. A noticeable observation is that the DMJ method exhibits a preference for heavier vector-like leptons (scalar) with larger coupling strengths when compared to the TD method, primarily due to its inclination for shorter lifetimes. Additionally, as the mass of the VLL increases, the projected sensitivities weaken, primarily attributable to the marked reduction in production cross-section. It is important to note that the left-side or right-side truncations in each plot arise from the dynamic requirement that necessitates m_F to be greater than m_ϕ . Overall, these results demonstrate that the combined utilization of these two methods can achieve sensitivity in the range of $y\theta_L$ from $\sim 10^{-11}$ to $\sim 10^{-6}$ for VLL masses within the range of $m_F \in [200, 1200]$

GeV. Throughout our calculations, we have taken $y = 1$ as an illustrative example to ensure that the decay $F \rightarrow \phi\ell$ is both prompt and dominant, while the pair production cross-section does not depend on y . The other values of y are also acceptable as long as the decay remains prompt and dominant.

It is important to highlight that when the mass of ϕ (m_ϕ) is close to the mass of the Z boson (m_Z), the invariant mass of the displaced or time-delayed dimuon, denoted as $m_{\mu_1\mu_2}$, will coincide with the region around the pole of the SM Z boson. This scenario carries intriguing implications. If ϕ decays rapidly, it can potentially result in an excess of dimuon events near the Z pole. This, in turn, offers a promising avenue for detecting the presence of ϕ with a mass in close proximity to that of the Z pole by making precise measurements of the Z boson. On the other hand, one might raise concerns about whether a similar mass range could significantly affect the primary decay channel of F^\pm . According to Eq. (9) and (13), the ratio of the two decay widths can be estimated as $\frac{\Gamma(F^- \rightarrow W^- \nu)}{\Gamma(F^- \rightarrow \phi \ell^-)} \sim \left(\frac{\theta_L}{y}\right)^2 \cdot \left(\frac{m_F}{m_W}\right)^2$, assuming the negligible lepton mass. In this context, this ratio is expected to be exceedingly small, thus ensuring that the decays of F remain unaffected.

C. Search for long-lived scalars at future CEPC

Other than the aforementioned searches at future hadronic collider HL-LHC, the latter case of long-live scalar can also be probed at the future e^-e^+ collider, such as CEPC [84], FCC-ee [85], and ILC [86], assuming that the F^\pm and ϕ exclusively mix with the first SM lepton generation. Here we take CEPC with center-of-mass energies $\sqrt{s} = 240$ GeV as an example. With similar parameters settings, the F^-F^+ pair production is forbidden due to $m_F > 200$ GeV, and the only possible phenomena are the $\phi\phi$ pair production by exchanging F^\pm via t channel, as shown in Fig. 6. The contributions from the diagrams of exchanging electrons can be neglected, due to the suppression from tiny θ_L . For the same reason, the cross-section of $\phi\gamma$ production is too small to be considered.

As elucidated in Section II B, the scalar ϕ is generated and subsequently decays into a pair of e^+e^- particles, leading to the manifestation of DV signatures at colliders due to its long-lived nature. Generally, the displaced vertex can be reconstructed in various detector components, including the inner tracker (IT), ECAL, HCAL, or muon spectrometer (MS), contingent upon the specific final state of its decay. In our particular scenario, featuring electronic final states ($\phi \rightarrow e^-e^+$), we exclusively employ the IT for the reconstruction of DV. This choice stems from the superior vertex

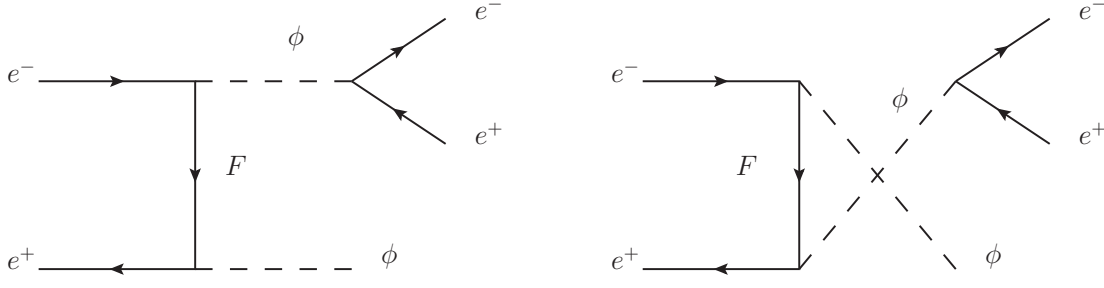


FIG. 6. The Feynman diagrams for the pair production and decay of the long-lived scalar ϕ at CEPC, where we neglect the diagrams of exchanging electrons because of tiny coupling θ_L .

reconstruction capabilities of the IT, while the ECAL and MS are less suitable for this purpose. Leveraging the efficient IT reconstruction, we implement an inclusive search strategy, stipulating the requirement for at least one reconstructed DV within the IT to confirm the identification of a signal event. The number of signal events can be expressed as:

$$N^{\text{IT}} = \mathcal{L}^{\text{CEPC}} \cdot \sigma(e^-e^+ \rightarrow \phi\phi) \cdot \langle \mathbb{P}_\phi^{\text{IT}} \rangle \cdot \epsilon^{\text{IT}}, \quad (48)$$

where $\mathcal{L}^{\text{CEPC}}$ is the integrated luminosity, $\sigma(e^-e^+ \rightarrow \phi\phi)$ is the cross-section of $\phi\phi$ pair production, and ϵ^{IT} is the other kinematic cut efficiency in the IT. The cross-section at the tree level can be formulated as

$$\sigma(e^-e^+ \rightarrow \phi\phi) = \frac{y^2}{64\pi s^2} \left[-3\sqrt{s(s-4m_\phi^2)} + \frac{2\left(s^2 + 2s(3m_F^2 - 2m_\phi^2) + 6(m_F^2 - m_\phi^2)^2\right) \tanh^{-1} \frac{\sqrt{s(s-4m_\phi^2)}}{s+2m_F^2-2m_\phi^2}}{s+2m_F^2-2m_\phi^2} \right]. \quad (49)$$

Moreover, the $\langle \mathbb{P}_\phi^{\text{IT}} \rangle$ denotes the average probability that at least one ϕ decays inside the IT where 100% detection efficiency is assumed. The average probability $\langle \mathbb{P}_\phi^{\text{IT}} \rangle$ can be expressed as [87]

$$\langle \mathbb{P}_\phi^{\text{IT}} \rangle = \frac{1}{N} \sum_{i=1}^N \left(\mathbb{P}_{\phi_i^1}^{\text{IT}} + \mathbb{P}_{\phi_i^2}^{\text{IT}} - \mathbb{P}_{\phi_i^1}^{\text{IT}} \cdot \mathbb{P}_{\phi_i^2}^{\text{IT}} \right), \quad (50)$$

where N denotes the total number of Monte Carlo events generated by MadGraph 5, and $\mathbb{P}_{\phi_i^j}^{\text{IT}}$ corresponds to the probability of the j th ϕ in the i th event decaying inside the IT. Generally, for a particle ϕ produced at the interaction point (IP) and along the direction of \vec{r}_ϕ , the probability of it decaying within a distance $d_\phi \in [r_\phi^1, r_\phi^2]$ from the IP is given by

$$\mathbb{P}_{\phi_i}^{\text{IT}} = \exp\left(-\frac{r_\phi^1}{\gamma_i \beta_i \tau(\phi)}\right) - \exp\left(-\frac{r_\phi^2}{\gamma_i \beta_i \tau(\phi)}\right), \quad (51)$$

where $\gamma_i \beta_i = \frac{E_i |\vec{p}_i|}{m_\phi E_i}$ is the Lorentz factor. In the center-of-mass frame, the two ϕ s produced by the collisions ($e^- e^+ \rightarrow \phi\phi$) hold the same magnitude momentum but opposite directions, so for axisymmetric detectors, the $\mathbb{P}_{\phi_i}^{\text{IT}}$ will be same for $i = 1$ and 2. Thus, the average probability in Eq. (50) can be reduced to

$$\langle \mathbb{P}_{\phi}^{\text{IT}} \rangle = \frac{1}{N} \sum_{i=1}^N \left(2\mathbb{P}_{\phi_i}^{\text{IT}} - \left(\mathbb{P}_{\phi_i}^{\text{IT}} \right)^2 \right). \quad (52)$$

Specific to the IT case, we require the displaced distance d_ϕ along its moving direction \vec{r}_ϕ to satisfy $10 \text{ cm} < |d_\phi \cdot \sin \theta_i| < 1.8 \text{ m}$ and $|d_\phi \cdot \cos \theta_i| < 2.35 \text{ m}$ with θ_i represents the angle between the ϕ of the i th event and the beam line axis [87, 88]. There has been the choice of $5 \text{ mm} < |d_\phi| < 1.22 \text{ m}$ with the assumption of a single background event [89], but for conservative, we choose the choice from Ref. [87]. This condition effectively suppresses the SM backgrounds from the prompt decays of Z or H bosons. In addition, we apply some kinematic cuts on the ee final states to further reduce the SM backgrounds. The complete selection criteria, including the displaced vertex condition, are listed as follows:

$$\begin{aligned} \text{DV-CEPC : } & 10 \text{ cm} < |d_\phi \cdot \sin \theta_i| < 1.8 \text{ m}, |d_\phi \cdot \cos \theta_i| < 2.35 \text{ m}, \\ & p_T^{e_i} > 30 \text{ GeV}, m_{e_1 e_2}(m_\phi) > 20 \text{ GeV}, 1 > \Delta R > 0.01, \end{aligned} \quad (53)$$

where p_T^e is the electron transverse momentum, ΔR denotes the opening angle of the two electrons from the ϕ decays, and the corresponding dedicated requirements on p_T and ΔR can effectively eliminate the SM backgrounds of heavier particles while maintaining good tracking spatial resolution [87]. Besides, by requiring the invariant mass $m_{e_1 e_2}(m_\phi)$ of the electron pair from the displaced vertex greater than 20 GeV, the possible backgrounds from the decays of long-lived SM hadrons or mesons ($\text{SM} \rightarrow e^- e^+$) can be further attenuated. With the displaced vertex, the SM background can be eliminated to a negligible level. Furthermore, we can impose both the two ϕ s vertices in each signal event to be displaced (2DV), which greatly reduces the only possible SM background from coincidences or misreconstructions. The average probability of 2DV similar to Eq. (52) can be expressed as

$$\langle \mathbb{P}_{\phi\phi}^{\text{IT}} \rangle = \frac{1}{N} \sum_{i=1}^N \left(\mathbb{P}_{\phi_i}^{\text{IT}} \cdot \mathbb{P}_{\phi_i}^{\text{IT}} \right) = \frac{1}{N} \sum_{i=1}^N \left(\mathbb{P}_{\phi_i}^{\text{IT}} \right)^2 \quad (54)$$

Similar to the case of detection in LHC, we divide our parameter space $\{m_F, m_\phi, \theta_L\}$ into three benchmarks: fixed m_F , fixed m_ϕ , and fixed ratio of m_F/m_ϕ . The corresponding sensitivities including the inclusive displaced vertex (iDV) and two displaced vertex (2DV) at future CEPC are shown in Fig. 7, with $\mathcal{L}^{\text{CEPC}} = 5.6 \text{ ab}^{-1}$ [88], where the number of signal events $N^{\text{IT}} = 3$ are plotted. It

is worth noting that the right-side truncation in the left and the right panel of Fig. 7 comes from a steep drop in cut efficiency, which is different from the feature of the DMJ methods at HL-LHC. This is due to the cuts on the opening angle ΔR , as the larger m_ϕ is, the velocity of ϕ becomes smaller, or ϕ becomes less boosted, so the angle between its decay products will be larger than 1, not fulfilling our selection criteria.

Moreover, compared to HL-LHC searches, the DV searches at CEPC can well probe the low-mass regions of the scalar ϕ but are incapable of detecting the large mass as a result of the low center-of-mass energy of CEPC. Nevertheless, with a higher integrated luminosity of 5.6 ab^{-1} , the CEPC shows better performance than HL-LHC. Besides, the inclusive displaced vertex searches completely cover the two displaced vertices, as expected. For $m_\phi \in [20, 70] \text{ GeV}$, a small coupling θ_L of $O(10^{-12}, 10^{-7})$ can be explored via the displaced vertex method in the future CEPC.

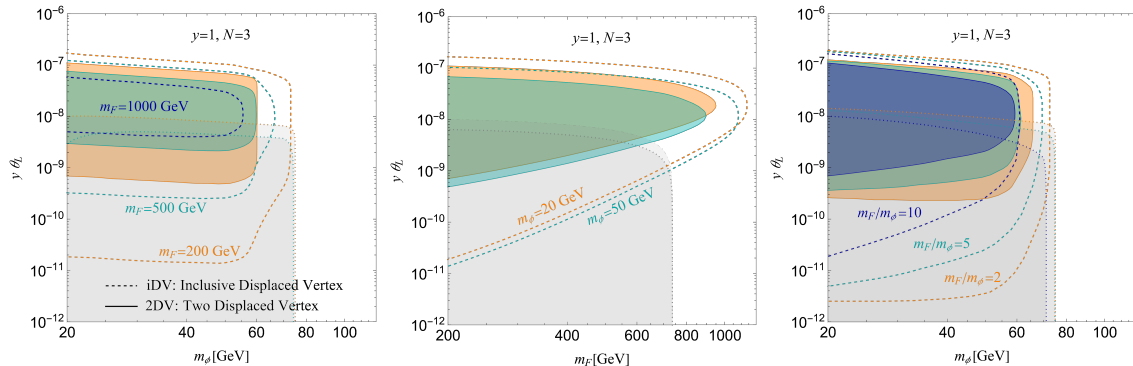


FIG. 7. The expected 95% C.L. sensitivities at Higgs factory of CEPC for the long-lived scalar case as a function of the scalar or vector-like lepton mass m_ϕ or m_F for $\mathcal{L} = 5.6 \text{ ab}^{-1}$ and $\sqrt{s} = 240 \text{ GeV}$. From left to right, the m_F fixed, m_ϕ fixed, and three mass ratios m_F/m_ϕ fixed cases are shown, respectively. The sensitivities for different masses of vector-like lepton m_F are shown with different colors, and the sensitivities from iDV (inclusive displaced vertex) and 2DV (two displaced vertex) search strategies are shown with dashed lines without color shading and with straight lines with color-shading, respectively. Moreover, the gray-shaded regions represent the constraints from LHC dilepton and missing energy or transverse momentum searches, with the corresponding colors as boundaries for different masses.

V. CONCLUSIONS

Vector-like leptons are a simple extension of the SM that have the same left- and right-handed transformations under gauge symmetry. They are usually classified by their corresponding coupled

SM lepton generation, which implies that they have the same quantum numbers as the SM leptons. Previous research has mainly focused on the prompt decays of the VLLs produced by electroweak processes. In this paper, we explore the potential long-lived signatures of VLLs or their subsequent decay products ϕ , which could leave a charged long-lived track or a displaced vertex in the detector. This provides a new way of probing heavier and weakly mixed VLLs.

We consider a generic model where a new $SU(2)_L$ singlet VLL mixes chirally with its corresponding charged SM right-handed lepton via a small mass mixing term. This chiral mass mixing induces naturally small and purely left-handed current interactions similar to the CC and NC interactions in SM. This motivates us to investigate its long-lived signatures. We then introduce two specific models. For the first one, we study the straightforward searches for the long-lived charged VLLs F^\pm at the ATLAS detector using the kink track method. We also examine experimental constraints from heavy stable charged particle searches, and dilepton plus missing energy (or transverse momentum) searches, which exclude regions with small couplings.

Secondly, we consider another model with an additional light scalar that has a sizable Yukawa interaction with the VLL. In this case, the long-lived signatures are transferred from the VLL to the scalar, which decays into an opposite-sign same-flavor muon pair, leaving a displaced vertex. Besides the current constraints from the multilepton searches at the LHC, we also perform searches for the long-lived scalars using the displaced muon-jet and time-delay methods. These two methods show good sensitivities for $m_F \in [200, 1200]$ GeV, with a moderate small coupling region around $10^{-11} < y\theta_L < 10^{-6}$. Moreover, we explore the long-lived signatures of the scalars at the future electron-positron collider such as CEPC, provided that the VLL couples to the first-generation SM leptons. We find that the CEPC has good performance for $m_\phi < 70$ GeV and $m_F < 1000$ GeV, using the displaced vertex method, due to the high luminosity of the future electron-positron collider. In conclusion, searching for the long-lived properties of VLLs or their accompanying scalars is a useful complement to previous prompt searches, as it reveals some distinctive and clean features.

VI. ACKNOWLEDGMENTS

We would like to thank Yuxuan He for his early verifying works and useful discussions. The work of QHC is supported in part by the National Science Foundation of China under Grants No. 11725520, No. 11675002, No. 12075257 and No. 12235001. The work of JL is supported by

Natural Science Foundation of China under grant No. 12075005 and 12235001. The work of XPW is supported by National Science Foundation of China under Grant No. 12005009, 12375095, and the Fundamental Research Funds for the Central Universities.

-
- [1] P. H. Frampton, P. Q. Hung, and M. Sher, *Quarks and leptons beyond the third generation*, Phys. Rept. **330** (2000) 263, [[hep-ph/9903387](#)].
- [2] F. Baspehlivan, B. Dagli, O. E. Delialioglu, and S. Sultansoy, *Why should we search for vector-like leptons?*, [arXiv:2201.08251](#).
- [3] **D0** Collaboration, V. M. Abazov et al., *Search for Single Vector-Like Quarks in $p\bar{p}$ Collisions at $\sqrt{s} = 1.96$ TeV*, Phys. Rev. Lett. **106** (2011) 081801, [[arXiv:1010.1466](#)].
- [4] **CDF** Collaboration, T. Aaltonen et al., *Search for New Bottomlike Quark Pair Decays $Q\bar{Q} \rightarrow (tW^\mp)(\bar{t}W^\pm)$ in Same-Charge Dilepton Events*, Phys. Rev. Lett. **104** (2010) 091801, [[arXiv:0912.1057](#)].
- [5] **CMS** Collaboration, S. Chatrchyan et al., *Search for a Vector-like Quark with Charge $2/3$ in $t + Z$ Events from pp Collisions at $\sqrt{s} = 7$ TeV*, Phys. Rev. Lett. **107** (2011) 271802, [[arXiv:1109.4985](#)].
- [6] **ATLAS** Collaboration, M. Aaboud et al., *Search for pair production of vector-like top quarks in events with one lepton, jets, and missing transverse momentum in $\sqrt{s} = 13$ TeV pp collisions with the ATLAS detector*, JHEP **08** (2017) 052, [[arXiv:1705.10751](#)].
- [7] **ATLAS** Collaboration, M. Aaboud et al., *Combination of the searches for pair-produced vector-like partners of the third-generation quarks at $\sqrt{s} = 13$ TeV with the ATLAS detector*, Phys. Rev. Lett. **121** (2018), no. 21 211801, [[arXiv:1808.02343](#)].
- [8] **CMS** Collaboration, A. M. Sirunyan et al., *Search for pair production of vectorlike quarks in the fully hadronic final state*, Phys. Rev. D **100** (2019), no. 7 072001, [[arXiv:1906.11903](#)].
- [9] **CMS** Collaboration, A. Tumasyan et al., *Search for pair production of vector-like quarks in leptonic final states in proton-proton collisions at $\sqrt{s} = 13$ TeV*, JHEP **07** (2023) 020, [[arXiv:2209.07327](#)].
- [10] **ATLAS** Collaboration, *Search for third-generation vector-like leptons in pp collisions at $\sqrt{s} = 13$ TeV with the ATLAS detector*, [arXiv:2303.05441](#).
- [11] **CMS** Collaboration, A. M. Sirunyan et al., *Search for vector-like leptons in multilepton final states in proton-proton collisions at $\sqrt{s} = 13$ TeV*, Phys. Rev. D **100** (2019), no. 5 052003, [[arXiv:1905.10853](#)].

- [12] CMS Collaboration, A. Tumasyan et al., *Inclusive nonresonant multilepton probes of new phenomena at $\sqrt{s}=13$ TeV*, Phys. Rev. D **105** (2022), no. 11 112007, [[arXiv:2202.08676](#)].
- [13] J. Muse, Search for third generation vector-like leptons with the ATLAS detector. PhD thesis, Oklahoma U., 2022.
- [14] S. D. Thomas and J. D. Wells, *Phenomenology of Massive Vectorlike Doublet Leptons*, Phys. Rev. Lett. **81** (1998) 34–37, [[hep-ph/9804359](#)].
- [15] M. Sher, *Charged leptons with nanosecond lifetimes*, Phys. Rev. D **52** (1995) 3136–3138, [[hep-ph/9504257](#)].
- [16] A. Falkowski, D. M. Straub, and A. Vicente, *Vector-like leptons: Higgs decays and collider phenomenology*, JHEP **05** (2014) 092, [[arXiv:1312.5329](#)].
- [17] P. N. Bhattiprolu and S. P. Martin, *Prospects for vectorlike leptons at future proton-proton colliders*, Phys. Rev. D **100** (2019), no. 1 015033, [[arXiv:1905.00498](#)].
- [18] N. F. Bell, M. J. Dolan, L. S. Friedrich, M. J. Ramsey-Musolf, and R. R. Volkas, *Electroweak Baryogenesis with Vector-like Leptons and Scalar Singlets*, JHEP **09** (2019) 012, [[arXiv:1903.11255](#)].
- [19] R. Dermisek, J. P. Hall, E. Lunghi, and S. Shin, *Limits on Vectorlike Leptons from Searches for Anomalous Production of Multi-Lepton Events*, JHEP **12** (2014) 013, [[arXiv:1408.3123](#)].
- [20] N. Kumar and S. P. Martin, *Vectorlike Leptons at the Large Hadron Collider*, Phys. Rev. D **92** (2015), no. 11 115018, [[arXiv:1510.03456](#)].
- [21] L. Shang, M. Wang, Z. Heng, and B. Yang, *Search for the singlet vector-like lepton at future e^+e^- colliders*, Eur. Phys. J. C **81** (2021), no. 5 415.
- [22] Q. Guo, L. Gao, Y. Mao, and Q. Li, *Vector-like lepton searches at a muon collider in the context of the 4321 model**, Chin. Phys. C **47** (2023), no. 10 103106, [[arXiv:2304.01885](#)].
- [23] J. Kearney, A. Pierce, and N. Weiner, *Vectorlike Fermions and Higgs Couplings*, Phys. Rev. D **86** (2012) 113005, [[arXiv:1207.7062](#)].
- [24] J. Halverson, N. Orlofsky, and A. Pierce, *Vectorlike Leptons as the Tip of the Dark Matter Iceberg*, Phys. Rev. D **90** (2014), no. 1 015002, [[arXiv:1403.1592](#)].
- [25] C. Arina, R. N. Mohapatra, and N. Sahu, *Co-genesis of Matter and Dark Matter with Vector-like Fourth Generation Leptons*, Phys. Lett. B **720** (2013) 130–136, [[arXiv:1211.0435](#)].
- [26] P. Schwaller, T. M. P. Tait, and R. Vega-Morales, *Dark Matter and Vectorlike Leptons from Gauged Lepton Number*, Phys. Rev. D **88** (2013), no. 3 035001, [[arXiv:1305.1108](#)].

- [27] R. Dermisek and A. Raval, *Explanation of the Muon $g-2$ Anomaly with Vectorlike Leptons and its Implications for Higgs Decays*, Phys. Rev. D **88** (2013) 013017, [[arXiv:1305.3522](#)].
- [28] K. Ishiwata and M. B. Wise, *Phenomenology of heavy vectorlike leptons*, Phys. Rev. D **88** (2013), no. 5 055009, [[arXiv:1307.1112](#)].
- [29] R. Dermisek, A. Raval, and S. Shin, *Effects of vectorlike leptons on $h \rightarrow 4\ell$ and the connection to the muon $g-2$ anomaly*, Phys. Rev. D **90** (2014), no. 3 034023, [[arXiv:1406.7018](#)].
- [30] R. Dermisek, E. Lunghi, and S. Shin, *Two Higgs doublet model with vectorlike leptons and contributions to $pp \rightarrow WW$ and $H \rightarrow WW$* , JHEP **02** (2016) 119, [[arXiv:1509.04292](#)].
- [31] C.-H. Chen and T. Nomura, *Bounds on LFV Higgs decays in a vector-like lepton model and searching for doubly charged leptons at the LHC*, Eur. Phys. J. C **76** (2016), no. 6 353, [[arXiv:1602.07519](#)].
- [32] Z. Poh and S. Raby, *Vectorlike leptons: Muon $g-2$ anomaly, lepton flavor violation, Higgs boson decays, and lepton nonuniversality*, Phys. Rev. D **96** (2017), no. 1 015032, [[arXiv:1705.07007](#)].
- [33] F.-Z. Xu, W. Zhang, J. Li, and T. Li, *Search for the vectorlike leptons in the $U(1)_X$ model inspired by the B -meson decay anomalies*, Phys. Rev. D **98** (2018), no. 11 115033, [[arXiv:1809.01472](#)].
- [34] S. Zheng, *Minimal Vectorlike Model in Supersymmetric Unification*, Eur. Phys. J. C **80** (2020), no. 3 273, [[arXiv:1904.10145](#)].
- [35] F. F. Freitas, J. a. Gonçalves, A. P. Morais, and R. Pasechnik, *Phenomenology of vector-like leptons with Deep Learning at the Large Hadron Collider*, JHEP **01** (2021) 076, [[arXiv:2010.01307](#)].
- [36] S. Bißmann, G. Hiller, C. Hormigos-Feliu, and D. F. Litim, *Multi-lepton signatures of vector-like leptons with flavor*, Eur. Phys. J. C **81** (2021), no. 2 101, [[arXiv:2011.12964](#)].
- [37] R. Dermisek, K. Hermanek, and N. McGinnis, *Muon $g-2$ in two-Higgs-doublet models with vectorlike leptons*, Phys. Rev. D **104** (2021), no. 5 055033, [[arXiv:2103.05645](#)].
- [38] J. Kawamura and S. Raby, *Signal of four muons or more from a vector-like lepton decaying to a muon-philic Z' boson at the LHC*, Phys. Rev. D **104** (2021), no. 3 035007, [[arXiv:2104.04461](#)].
- [39] B. Yang, J. Li, M. Wang, and L. Shang, *Search for the singlet vectorlike lepton in semileptonic channel at future e^+e^- colliders*, Phys. Rev. D **104** (2021), no. 5 055019.
- [40] H. Li, J. Chao, and G. Zhang, *Search for the singlet vector-like lepton in $W\nu\tau$ channel at the TeV e^+e^- colliders*, Int. J. Mod. Phys. A **37** (2022), no. 36 2250224.
- [41] M. Raju, A. Mukherjee, and J. P. Saha, *Investigation of $(g-2)_\mu$ anomaly in the μ -specific 2HDM with vector like leptons and the phenomenological implications*, Eur. Phys. J. C **83** (2023), no. 5 429, [[arXiv:2207.02825](#)].

- [42] H. Li, J. Chao, and G. Zhang, *Search for the singlet vector-like lepton through the pair production in the $W\nu_\tau$ channel at the ILC*, EPL **139** (2022), no. 6 64001.
- [43] L. Shang, J. Li, X. Jia, and B. Yang, *Search for Pair-Produced vectorlike lepton singlet at the ILC by the XGBoost method*, Nucl. Phys. B **987** (2023) 116071.
- [44] J. Kawamura and S. Shin, *Current status on pair-produced muon-philic vectorlike leptons in multilepton channels at the LHC*, [arXiv:2308.07814](#).
- [45] P. N. Bhattiprolu, S. P. Martin, and A. Pierce, *Isosinglet vectorlike leptons at e^+e^- colliders*, [arXiv:2308.08386](#).
- [46] P. Bandyopadhyay, M. Frank, S. Parashar, and C. Sen, *Interplay of inert doublet and vector-like lepton triplet with displaced vertices at the LHC/FCC and MATHUSLA*, [arXiv:2310.08883](#).
- [47] E. Bernreuther and B. A. Dobrescu, *Vectorlike leptons and long-lived bosons at the LHC*, JHEP **07** (2023) 079, [[arXiv:2304.08509](#)].
- [48] CMS Collaboration, S. Chatrchyan et al., *Searches for Long-Lived Charged Particles in pp Collisions at $\sqrt{s}=7$ and 8 TeV*, JHEP **07** (2013) 122, [[arXiv:1305.0491](#)]. [Erratum: JHEP 11, 149 (2022)].
- [49] CMS Collaboration, *Search for heavy stable charged particles with 12.9 fb^{-1} of 2016 data*, .
- [50] CMS Collaboration, A. M. Sirunyan et al., *Performance of the CMS muon trigger system in proton-proton collisions at $\sqrt{s} = 13\text{ TeV}$* , JINST **16** (2021) P07001, [[arXiv:2102.04790](#)].
- [51] ATLAS Collaboration, G. Aad et al., *Search for electroweak production of charginos and sleptons decaying into final states with two leptons and missing transverse momentum in $\sqrt{s} = 13\text{ TeV}$ pp collisions using the ATLAS detector*, Eur. Phys. J. C **80** (2020), no. 2 123, [[arXiv:1908.08215](#)].
- [52] CMS Collaboration, A. M. Sirunyan et al., *Search for supersymmetry in final states with two oppositely charged same-flavor leptons and missing transverse momentum in proton-proton collisions at $\sqrt{s} = 13\text{ TeV}$* , JHEP **04** (2021) 123, [[arXiv:2012.08600](#)].
- [53] J. Alwall, R. Frederix, S. Frixione, V. Hirschi, F. Maltoni, O. Mattelaer, H. S. Shao, T. Stelzer, P. Torrielli, and M. Zaro, *The automated computation of tree-level and next-to-leading order differential cross sections, and their matching to parton shower simulations*, JHEP **07** (2014) 079, [[arXiv:1405.0301](#)].
- [54] ATLAS Collaboration, G. Aad et al., *Search for new phenomena in three- or four-lepton events in pp collisions at $\sqrt{s}=13\text{ TeV}$ with the ATLAS detector*, Phys. Lett. B **824** (2022) 136832, [[arXiv:2107.00404](#)].

- [55] M. Ardu and G. Pezzullo, *Introduction to Charged Lepton Flavor Violation*, Universe **8** (2022), no. 6 299, [[arXiv:2204.08220](#)].
- [56] **MEG** Collaboration, A. M. Baldini et al., *Search for the lepton flavour violating decay $\mu^+ \rightarrow e^+\gamma$ with the full dataset of the MEG experiment*, Eur. Phys. J. C **76** (2016), no. 8 434, [[arXiv:1605.05081](#)].
- [57] **SINDRUM** Collaboration, U. Bellgardt et al., *Search for the Decay $\mu^+ \rightarrow e^+ e^+ e^-$* , Nucl. Phys. B **299** (1988) 1–6.
- [58] **BaBar** Collaboration, B. Aubert et al., *Searches for Lepton Flavor Violation in the Decays $\tau^{\pm} \rightarrow e^{\pm} \gamma$ and $\tau^{\pm} \rightarrow \mu^{\pm} \gamma$* , Phys. Rev. Lett. **104** (2010) 021802, [[arXiv:0908.2381](#)].
- [59] K. Hayasaka et al., *Search for Lepton Flavor Violating Tau Decays into Three Leptons with 719 Million Produced $\tau^+\tau^-$ Pairs*, Phys. Lett. B **687** (2010) 139–143, [[arXiv:1001.3221](#)].
- [60] X. G. He, G. C. Joshi, H. Lew, and R. R. Volkas, *NEW Z-prime PHENOMENOLOGY*, Phys. Rev. D **43** (1991) 22–24.
- [61] D. Hanneke, S. Fogwell, and G. Gabrielse, *New Measurement of the Electron Magnetic Moment and the Fine Structure Constant*, Phys. Rev. Lett. **100** (2008) 120801, [[arXiv:0801.1134](#)].
- [62] L. Morel, Z. Yao, P. Cladé, and S. Guellati-Khélifa, *Determination of the fine-structure constant with an accuracy of 81 parts per trillion*, Nature **588** (2020), no. 7836 61–65.
- [63] **Muon g-2** Collaboration, D. P. Aguillard et al., *Measurement of the Positive Muon Anomalous Magnetic Moment to 0.20 ppm*, Phys. Rev. Lett. **131** (2023), no. 16 161802, [[arXiv:2308.06230](#)].
- [64] D. Borah, S. Mahapatra, P. K. Paul, and N. Sahu, *Scotogenic $U(1)_{L_\mu-L_\tau}$ origin of $(g-2)_\mu$, W -mass anomaly and 95 GeV excess*, [arXiv:2310.11953](#).
- [65] **CMS** Collaboration, T. Reis, *Search for new Resonances in Dielectron and Dimuon Mass Spectra at $\sqrt{s} = 8$ TeV with CMS*, Nucl. Part. Phys. Proc. **273-275** (2016) 2433–2435.
- [66] **CMS** Collaboration, J. Tucker, *Search for narrow resonances in the dielectron and dimuon final states with CMS*, PoS EPS-HEP2011 (2011) 223.
- [67] S. Asai, Y. Azuma, M. Endo, K. Hamaguchi, and S. Iwamoto, *Stau Kinks at the LHC*, JHEP **12** (2011) 041, [[arXiv:1103.1881](#)].
- [68] D. Acosta et al., *Review of opportunities for new long-lived particle triggers in Run 3 of the Large Hadron Collider*, [arXiv:2110.14675](#).
- [69] **CMS Collaboration** Collaboration, T. A. collaboration, *The Phase-2 Upgrade of the CMS L1 Trigger Interim Technical Design Report*, tech. rep., CERN, Geneva, Sep, 2017. This is the CMS

Interim TDR devoted to the upgrade of the CMS L1 trigger in view of the HL-LHC running, as approved by the LHCC.

- [70] **ATLAS Collaboration** Collaboration, *Trigger menu in 2018*, tech. rep., CERN, Geneva, Oct, 2019. All figures including auxiliary figures are available at <https://atlas.web.cern.ch/Atlas/GROUPS/PHYSICS/PUBNOTES/ATL-DAQ-PUB-2019-001>.
- [71] A. Berlin and F. Kling, *Inelastic Dark Matter at the LHC Lifetime Frontier: ATLAS, CMS, LHCb, CODEX-b, FASER, and MATHUSLA*, Phys. Rev. D **99** (2019), no. 1 015021, [[arXiv:1810.01879](#)].
- [72] E. Izaguirre, G. Krnjaic, and B. Shuve, *Discovering Inelastic Thermal-Relic Dark Matter at Colliders*, Phys. Rev. D **93** (2016), no. 6 063523, [[arXiv:1508.03050](#)].
- [73] **CMS Collaboration** Collaboration, *Technical proposal for a MIP timing detector in the CMS experiment Phase 2 upgrade*, tech. rep., CERN, Geneva, Dec, 2017.
- [74] D. Contardo, M. Klute, J. Mans, L. Silvestris, and J. Butler, *Technical Proposal for the Phase-II Upgrade of the CMS Detector*, tech. rep., Geneva, Jun, 2015. Upgrade Project Leader Deputies: Lucia Silvestris (INFN-Bari), Jeremy Mans (University of Minnesota) Additional contacts: Lucia.Silvestris@cern.ch, Jeremy.Mans@cern.ch.
- [75] C. Allaire et al., *Beam test measurements of Low Gain Avalanche Detector single pads and arrays for the ATLAS High Granularity Timing Detector*, JINST **13** (2018), no. 06 P06017, [[arXiv:1804.00622](#)].
- [76] **LHCb** Collaboration, R. Aaij et al., *Physics case for an LHCb Upgrade II - Opportunities in flavour physics, and beyond, in the HL-LHC era*, [arXiv:1808.08865](#).
- [77] J. P. Chou, D. Curtin, and H. J. Lubatti, *New Detectors to Explore the Lifetime Frontier*, Phys. Lett. B **767** (2017) 29–36, [[arXiv:1606.06298](#)].
- [78] D. Curtin et al., *Long-Lived Particles at the Energy Frontier: The MATHUSLA Physics Case*, Rept. Prog. Phys. **82** (2019), no. 11 116201, [[arXiv:1806.07396](#)].
- [79] F. Kling and S. Trojanowski, *Heavy Neutral Leptons at FASER*, Phys. Rev. D **97** (2018), no. 9 095016, [[arXiv:1801.08947](#)].
- [80] J. L. Feng, I. Galon, F. Kling, and S. Trojanowski, *ForwArd Search ExpeRiment at the LHC*, Phys. Rev. D **97** (2018), no. 3 035001, [[arXiv:1708.09389](#)].
- [81] V. V. Gligorov, S. Knapen, M. Papucci, and D. J. Robinson, *Searching for Long-lived Particles: A Compact Detector for Exotics at LHCb*, Phys. Rev. D **97** (2018), no. 1 015023, [[arXiv:1708.09395](#)].

- [82] J. Liu, Z. Liu, and L.-T. Wang, *Enhancing Long-Lived Particles Searches at the LHC with Precision Timing Information*, Phys. Rev. Lett. **122** (2019), no. 13 131801, [[arXiv:1805.05957](#)].
- [83] J. Guo, Y. He, J. Liu, and X.-P. Wang, *Heavy long-lived coannihilation partner from inelastic Dark Matter model and its signatures at the LHC*, JHEP **04** (2022) 024, [[arXiv:2111.01164](#)].
- [84] M. Ahmad et al., *CEPC-SPPC Preliminary Conceptual Design Report. 1. Physics and Detector*, .
- [85] W. Venturini Delsolaro et al., *Progress and R/D challenges for FCC-ee SRF*, EPJ Tech. Instrum. **10** (2023), no. 1 6.
- [86] **ILC** Collaboration, G. Aarons et al., *International Linear Collider Reference Design Report Volume 2: Physics at the ILC*, [arXiv:0709.1893](#).
- [87] K. Cheung and Z. S. Wang, *Probing Long-lived Particles at Higgs Factories*, Phys. Rev. D **101** (2020), no. 3 035003, [[arXiv:1911.08721](#)].
- [88] **CEPC Study Group** Collaboration, M. Dong et al., *CEPC Conceptual Design Report: Volume 2 - Physics & Detector*, [arXiv:1811.10545](#).
- [89] M. Chrzęszcz, M. Drewes, and J. Hajer, *HECATE: A long-lived particle detector concept for the FCC-ee or CEPC*, Eur. Phys. J. C **81** (2021), no. 6 546, [[arXiv:2011.01005](#)].